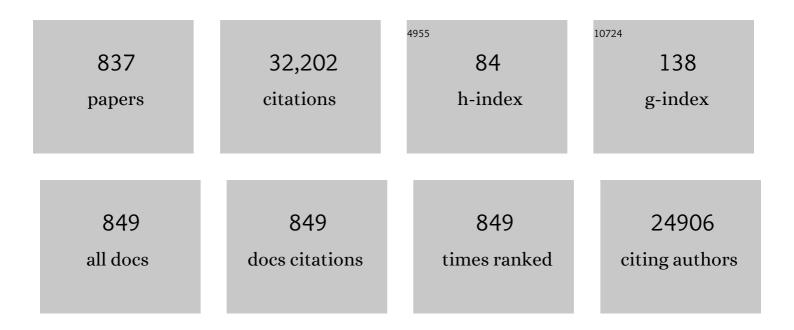
List of Publications by Year in descending order

Source: https://exaly.com/author-pdf/2417872/publications.pdf Version: 2024-02-01



ROBERT M HOEEMAN

#	Article	IF	CITATIONS
1	Physical limits of cell migration: Control by ECM space and nuclear deformation and tuning by proteolysis and traction force. Journal of Cell Biology, 2013, 201, 1069-1084.	2.3	1,123
2	A Senescence Program Controlled by p53 and p16INK4a Contributes to the Outcome of Cancer Therapy. Cell, 2002, 109, 335-346.	13.5	966
3	The multiple uses of fluorescent proteins to visualize cancer in vivo. Nature Reviews Cancer, 2005, 5, 796-806.	12.8	582
4	Orthotopic metastatic mouse models for anticancer drug discovery and evaluation: a bridge to the clinic. , 1999, 17, 343-360.		495
5	Transdifferentiation of glioblastoma cells into vascular endothelial cells. Proceedings of the National Academy of Sciences of the United States of America, 2011, 108, 4274-4280.	3.3	484
6	Dissecting p53 tumor suppressor functions in vivo. Cancer Cell, 2002, 1, 289-298.	7.7	478
7	Tumor-targeting bacterial therapy with amino acid auxotrophs of GFP-expressing Salmonella typhimurium. Proceedings of the National Academy of Sciences of the United States of America, 2005, 102, 755-760.	3.3	439
8	Gene expression profiling predicts clinical outcome of prostate cancer. Journal of Clinical Investigation, 2004, 113, 913-923.	3.9	405
9	Multipotent nestin-positive, keratin-negative hair-follicle bulge stem cells can form neurons. Proceedings of the National Academy of Sciences of the United States of America, 2005, 102, 5530-5534.	3.3	404
10	Patient-derived orthotopic xenografts: better mimic of metastasis than subcutaneous xenografts. Nature Reviews Cancer, 2015, 15, 451-452.	12.8	361
11	Nestin expression in hair follicle sheath progenitor cells. Proceedings of the National Academy of Sciences of the United States of America, 2003, 100, 9958-9961.	3.3	333
12	Implanted hair follicle stem cells form Schwann cells that support repair of severed peripheral nerves. Proceedings of the National Academy of Sciences of the United States of America, 2005, 102, 17734-17738.	3.3	315
13	Targeted Therapy with a Salmonella Typhimurium Leucine-Arginine Auxotroph Cures Orthotopic Human Breast Tumors in Nude Mice. Cancer Research, 2006, 66, 7647-7652.	0.4	278
14	lmaging exosome transfer from breast cancer cells to stroma at metastatic sites in orthotopic nude-mouse models. Advanced Drug Delivery Reviews, 2013, 65, 383-390.	6.6	267
15	Development of Real-time Subcellular Dynamic Multicolor Imaging of Cancer-Cell Trafficking in Live Mice with a Variable-Magnification Whole-Mouse Imaging System. Cancer Research, 2006, 66, 4208-4214.	0.4	242
16	Green fluorescent protein imaging of tumour growth, metastasis, and angiogenesis in mouse models. Lancet Oncology, The, 2002, 3, 546-556.	5.1	232
17	Monotherapy with a tumor-targeting mutant of Salmonella typhimurium cures orthotopic metastatic mouse models of human prostate cancer. Proceedings of the National Academy of Sciences of the United States of America, 2007, 104, 10170-10174.	3.3	229
18	Increased Expression of Apoptosis Inhibitor Protein XIAP Contributes to Anoikis Resistance of Circulating Human Prostate Cancer Metastasis Precursor Cells. Cancer Research, 2005, 65, 2378-2386.	0.4	218

#	Article	IF	CITATIONS
19	Nascent blood vessels in the skin arise from nestin-expressing hair-follicle cells. Proceedings of the National Academy of Sciences of the United States of America, 2004, 101, 13291-13295.	3.3	215
20	The feasibility of targeted selective gene therapy of the hair follicle. Nature Medicine, 1995, 1, 705-706.	15.2	209
21	Potent and Highly Selective Hypoxia-Activated Achiral Phosphoramidate Mustards as Anticancer Drugs. Journal of Medicinal Chemistry, 2008, 51, 2412-2420.	2.9	208
22	Dual-color fluorescence imaging distinguishes tumor cells from induced host angiogenic vessels and stromal cells. Proceedings of the National Academy of Sciences of the United States of America, 2003, 100, 14259-14262.	3.3	188
23	The metabolic defect of methionine dependence occurs frequently in human tumor cell lines. Biochemical and Biophysical Research Communications, 1983, 117, 429-434.	1.0	184
24	Whole-body imaging with fluorescent proteins. Nature Protocols, 2006, 1, 1429-1438.	5.5	183
25	Direct external imaging of nascent cancer, tumor progression, angiogenesis, and metastasis on internal organs in the fluorescent orthotopic model. Proceedings of the National Academy of Sciences of the United States of America, 2002, 99, 3824-3829.	3.3	179
26	Real-time In vivo Dual-color Imaging of Intracapillary Cancer Cell and Nucleus Deformation and Migration. Cancer Research, 2005, 65, 4246-4252.	0.4	160
27	Subcellular imaging in the live mouse. Nature Protocols, 2006, 1, 775-782.	5.5	160
28	Altered methionine metabolism occurs in all members of a set of diverse human tumor cell lines. Journal of Cellular Physiology, 1984, 119, 29-34.	2.0	158
29	Color-coded fluorescence imaging of tumor-host interactions. Nature Protocols, 2006, 1, 928-935.	5.5	157
30	Essential Role for Activation of the Polycomb Group (PcG) Protein Chromatin Silencing Pathway in Metastatic Prostate Cancer. Cell Cycle, 2006, 5, 1886-1901.	1.3	150
31	Peptides selected for binding to clotted plasma accumulate in tumor stroma and wounds. Proceedings of the National Academy of Sciences of the United States of America, 2006, 103, 2800-2804.	3.3	150
32	Multipotent hair follicle stem cells promote repair of spinal cord injury and recovery of walking function. Cell Cycle, 2008, 7, 1865-1869.	1.3	150
33	Altered methionine metabolism, DNA methylation and oncogene expression in carcinogenesis. Biochimica Et Biophysica Acta: Reviews on Cancer, 1984, 738, 49-87.	3.3	148
34	Overexpression and Large-Scale Production of Recombinantl-Methionine-α-deamino-γ-mercaptomethane-lyase for Novel Anticancer Therapy. Protein Expression and Purification, 1997, 9, 233-245.	0.6	144
35	Overactivated Neddylation Pathway as a Therapeutic Target in Lung Cancer. Journal of the National Cancer Institute, 2014, 106, dju083.	3.0	144
36	Cellular Dynamics Visualized in Live Cells in Vitro and in Vivo by Differential Dual-Color Nuclear-Cytoplasmic Fluorescent-Protein Expression. Cancer Research, 2004, 64, 4251-4256.	0.4	141

#	Article	IF	CITATIONS
37	Real-time optical imaging of primary tumor growth and multiple metastatic events in a pancreatic cancer orthotopic model. Cancer Research, 2002, 62, 1534-40.	0.4	141
38	Nestin-Linked Green Fluorescent Protein Transgenic Nude Mouse for Imaging Human Tumor Angiogenesis. Cancer Research, 2005, 65, 5352-5357.	0.4	139
39	Orthotopic transplantation of histologically intact clinical specimens of stomach cancer to nude mice: Correlation of metastatic sites in mouse and individual patient donors. International Journal of Cancer, 1993, 53, 608-612.	2.3	138
40	In vivo internal tumor illumination by telomerase-dependent adenoviral GFP for precise surgical navigation. Proceedings of the National Academy of Sciences of the United States of America, 2009, 106, 14514-14517.	3.3	134
41	Fluorophore-conjugated anti-CEA Antibody for the Intraoperative Imaging of Pancreatic and Colorectal Cancer. Journal of Gastrointestinal Surgery, 2008, 12, 1938-1950.	0.9	133
42	Development of recombinant methioninase to target the general cancer-specific metabolic defect of methionine dependence: a 40-year odyssey. Expert Opinion on Biological Therapy, 2015, 15, 21-31.	1.4	133
43	A novel red fluorescent protein orthotopic pancreatic cancer model for the preclinical evaluation of chemotherapeutics. Journal of Surgical Research, 2003, 113, 151-160.	0.8	132
44	Fluorescently labeled chimeric antiâ€CEA antibody improves detection and resection of human colon cancer in a patientâ€derived orthotopic xenograft (PDOX) nude mouse model. Journal of Surgical Oncology, 2014, 109, 451-458.	0.8	132
45	Elevated overall rates of transmethylation in cell lines from diverse human tumors. In Vitro, 1984, 20, 663-670.	1.2	129
46	Transgenic Nude Mouse with Ubiquitous Green Fluorescent Protein Expression as a Host for Human Tumors. Cancer Research, 2004, 64, 8651-8656.	0.4	129
47	Efficacy of tumor-targeting Salmonella typhimurium A1-R in combination with anti-angiogenesis therapy on a pancreatic cancer patient-derived orthotopic xenograft (PDOX) and cell line mouse models. Oncotarget, 2014, 5, 12346-12357.	0.8	128
48	CXCâ€chemokine/CXCR2 biological axis promotes angiogenesis <i>in vitro</i> and <i>in vivo</i> in pancreatic cancer. International Journal of Cancer, 2009, 125, 1027-1037.	2.3	127
49	Characterization of HCT116 Human Colon Cancer Cells in an Orthotopic Model. Journal of Surgical Research, 2008, 147, 276-281.	0.8	125
50	Cancer metastasis directly eradicated by targeted therapy with a modified <i>Salmonella typhimurium</i> . Journal of Cellular Biochemistry, 2009, 106, 992-998.	1.2	125
51	Monotherapy with a Tumor-Targeting Mutant of S. typhimurium Inhibits Liver Metastasis in a Mouse Model of Pancreatic Cancer. Journal of Surgical Research, 2010, 164, 248-255.	0.8	125
52	In vitro sensitivity assays in cancer: A review, analysis, and prognosis. Journal of Clinical Laboratory Analysis, 1991, 5, 133-143.	0.9	122
53	Human hair follicle pluripotent stem (hfPS) cells promote regeneration of peripheralâ€nerve injury: An advantageous alternative to ES and iPS cells. Journal of Cellular Biochemistry, 2009, 107, 1016-1020.	1.2	119
54	Real-time Imaging of Tumor-Cell Shedding and Trafficking in Lymphatic Channels. Cancer Research, 2007, 67, 8223-8228.	0.4	118

#	Article	IF	CITATIONS
55	The bulge area is the origin of nestin-expressing pluripotent stem cells of the hair follicle. Journal of Cellular Biochemistry, 2011, 112, 2046-2050.	1.2	118
56	Whole-Body Subcellular Multicolor Imaging of Tumor-Host Interaction and Drug Response in Real Time. Cancer Research, 2007, 67, 5195-5200.	0.4	117
57	Successful Fluorescence-Guided Surgery on Human Colon Cancer Patient-Derived Orthotopic Xenograft Mouse Models Using a Fluorophore-Conjugated Anti-CEA Antibody and a Portable Imaging System. Journal of Laparoendoscopic and Advanced Surgical Techniques - Part A, 2014, 24, 241-247.	0.5	117
58	Induction of Cancer Metastasis by Cyclophosphamide Pretreatment of Host Mice: An Opposite Effect of Chemotherapy. Cancer Research, 2008, 68, 516-520.	0.4	115
59	Prolonged dormancy and site-specific growth potential of cancer cells spontaneously disseminated from nonmetastatic breast tumors as revealed by labeling with green fluorescent protein. Clinical Cancer Research, 2003, 9, 3808-14.	3.2	115
60	Role of the tumor microenvironment in pancreatic cancer. Annals of Gastroenterological Surgery, 2019, 3, 130-137.	1.2	114
61	Systemic targeting of primary bone tumor and lung metastasis of high-grade osteosarcoma in nude mice with a tumor-selective strain of <i>Salmonella typhymurium</i> . Cell Cycle, 2009, 8, 870-875.	1.3	113
62	To do tissue culture in two or three dimensions? that is the question. Stem Cells, 1993, 11, 105-111.	1.4	112
63	Tumor-targeting <i>Salmonella typhimurium</i> A1-R in combination with doxorubicin eradicate soft tissue sarcoma in a patient-derived orthotopic xenograft (PDOX) model. Oncotarget, 2016, 7, 12783-12790.	0.8	109
64	White paper on microbial anti-cancer therapy and prevention. , 2018, 6, 78.		108
65	Efficacy of a genetically-modified Salmonella typhimurium in an orthotopic human pancreatic cancer in nude mice. Anticancer Research, 2009, 29, 1873-8.	0.5	106
66	PEGylation Confers Greatly Extended Half-Life and Attenuated Immunogenicity to Recombinant Methioninase in Primates. Cancer Research, 2004, 64, 6673-6678.	0.4	105
67	In vivo Color-Coded Imaging of the Interaction of Colon Cancer Cells and Splenocytes in the Formation of Liver Metastases. Cancer Research, 2006, 66, 11293-11297.	0.4	105
68	Establishment of a Patient-Derived Orthotopic Xenograft (PDOX) Model of HER-2-Positive Cervical Cancer Expressing the Clinical Metastatic Pattern. PLoS ONE, 2015, 10, e0117417.	1.1	105
69	Pseudopodium-enriched atypical kinase 1 regulates the cytoskeleton and cancer progression. Proceedings of the National Academy of Sciences of the United States of America, 2010, 107, 10920-10925.	3.3	104
70	A transgenic red fluorescent proteinâ€expressing nude mouse for colorâ€eoded imaging of the tumor microenvironment. Journal of Cellular Biochemistry, 2009, 106, 279-284.	1.2	103
71	Enhanced In Vitro Selective Toxicity of Chemotherapeutic Agents for Human Cancer Cells Based on a Metabolic Defect2. Journal of the National Cancer Institute, 1986, 76, 629-639.	3.0	102
72	The bulge area is the major hair follicle source of nestin-expressing pluripotent stem cells which can repair the spinal cord compared to the dermal papilla. Cell Cycle, 2011, 10, 830-839.	1.3	101

#	Article	IF	CITATIONS
73	Vessel destruction by tumor-targeting <i>Salmonella typhimurium</i> A1-R is enhanced by high tumor vascularity. Cell Cycle, 2010, 9, 4518-4524.	1.3	99
74	Pancreatic cancer-derived exosomes promote tumor metastasis and liver pre-metastatic niche formation. Oncotarget, 2017, 8, 63461-63483.	0.8	98
75	Bacterial Therapy of Cancer: Promises, Limitations, and Insights for Future Directions. Frontiers in Microbiology, 2018, 9, 16.	1.5	98
76	The Pluripotency of Hair Follicle Stem Cells. Cell Cycle, 2006, 5, 232-233.	1.3	97
77	KRas Induces a Src/PEAK1/ErbB2 Kinase Amplification Loop That Drives Metastatic Growth and Therapy Resistance in Pancreatic Cancer. Cancer Research, 2012, 72, 2554-2564.	0.4	96
78	Tumor-targeting <i>Salmonella typhimurium</i> A1-R decoys quiescent cancer cells to cycle as visualized by FUCCI imaging and become sensitive to chemotherapy. Cell Cycle, 2014, 13, 3958-3963.	1.3	96
79	Neddylation Inhibition Activates the Extrinsic Apoptosis Pathway through ATF4–CHOP–DR5 Axis in Human Esophageal Cancer Cells. Clinical Cancer Research, 2016, 22, 4145-4157.	3.2	96
80	Targeting the Lymphotoxin-β Receptor with Agonist Antibodies as a Potential Cancer Therapy. Cancer Research, 2006, 66, 9617-9624.	0.4	95
81	Imaging of Primary and Metastatic Pancreatic Cancer Using a Fluorophore onjugated Anti A19â€9 Antibody for Surgical Navigation. World Journal of Surgery, 2008, 32, 1057-1066.	0.8	94
82	Efficacy of <i>Salmonella typhimurium</i> A1â€R Versus Chemotherapy on a Pancreatic Cancer Patientâ€Đerived Orthotopic Xenograft (PDOX). Journal of Cellular Biochemistry, 2014, 115, 1254-1261.	1.2	93
83	Efficacy of Tumor-Targeting Salmonella A1-R on a Melanoma Patient-Derived Orthotopic Xenograft (PDOX) Nude-Mouse Model. PLoS ONE, 2016, 11, e0160882.	1.1	93
84	High efficacy of tumor-targeting <i>Salmonella typhimurium</i> A1-R on a doxorubicin- and dactolisib-resistant follicular dendritic-cell sarcoma in a patient-derived orthotopic xenograft PDOX nude mouse model. Oncotarget, 2016, 7, 33046-33054.	0.8	93
85	Effective molecular targeting of CDK4/6 and IGF-1R in a rare <i>FUS-ERG</i> fusion <i>CDKN2A</i> -deletion doxorubicin-resistant Ewing's sarcoma patient-derived orthotopic xenograft (PDOX) nude-mouse model. Oncotarget, 2016, 7, 47556-47564.	0.8	91
86	The challenges posed by cancer heterogeneity. Nature Biotechnology, 2012, 30, 604-610.	9.4	90
87	Selective methioninase-induced trap of cancer cells in S/G2 phase visualized by FUCCI imaging confers chemosensitivity. Oncotarget, 2014, 5, 8729-8736.	0.8	85
88	Topical Liposome Targeting of Dyes, Melanins, Genes, and Proteins Selectively to Hair Follicles. Journal of Drug Targeting, 1998, 5, 67-74.	2.1	84
89	Knockdown of the β <sub>1</sub> integrin subunit reduces primary tumor growth and inhibits pancreatic cancer metastasis. International Journal of Cancer, 2011, 129, 2905-2915.	2.3	82
90	Metastatic Recurrence in a Pancreatic Cancer Patient Derived Orthotopic Xenograft (PDOX) Nude Mouse Model Is Inhibited by Neoadjuvant Chemotherapy in Combination with Fluorescence-Guided Surgery with an Anti-CA 19-9-Conjugated Fluorophore. PLoS ONE, 2014, 9, e114310.	1.1	82

#	Article	IF	CITATIONS
91	Fluorescence imaging of multiple myeloma cells in a clinically relevant SCID/NOD in vivo model: biologic and clinical implications. Cancer Research, 2003, 63, 6689-96.	0.4	81
92	Genistein inhibits the growth of human-patient BPH and prostate cancer in histoculture. , 1998, 34, 75-79.		80
93	Inhibition and eradication of human glioma with tumor-targeting <i>Salmonella typhimurium</i> in an orthotopic nude-mouse model. Cell Cycle, 2012, 11, 628-632.	1.3	80
94	Application of GFP imaging in cancer. Laboratory Investigation, 2015, 95, 432-452.	1.7	80
95	Highin vitro-in vivo correlation of drug response using sponge-gel-supported three-dimensional histoculture and the MTT end point. International Journal of Cancer, 1992, 51, 489-498.	2.3	79
96	Comparison of efficacy ofSalmonella typhimuriumA1-R and chemotherapy on stem-like and non-stem human pancreatic cancer cells. Cell Cycle, 2013, 12, 2774-2780.	1.3	78
97	Tumor-Targeting Salmonella typhimurium A1-R Arrests a Chemo-Resistant Patient Soft-Tissue Sarcoma in Nude Mice. PLoS ONE, 2015, 10, e0134324.	1.1	78
98	Tumor-targeting <i>Salmonella typhimurium</i> A1-R combined with temozolomide regresses malignant melanoma with a BRAF-V600E mutation in a patient-derived orthotopic xenograft (PDOX) model. Oncotarget, 2016, 7, 85929-85936.	0.8	77
99	Recombinant methioninase effectively targets a Ewing's sarcoma in a patient-derived orthotopic xenograft (PDOX) nude-mouse model. Oncotarget, 2017, 8, 35630-35638.	0.8	77
100	Fluorescence-guided Surgery with a Fluorophore-conjugated Antibody to Carcinoembryonic Antigen (CEA), that Highlights the Tumor, Improves Surgical Resection and Increases Survival in Orthotopic Mouse Models of Human Pancreatic Cancer. Annals of Surgical Oncology, 2014, 21, 1405-1411.	0.7	76
101	On the role of classical and novel forms of vitamin D in melanoma progression and management. Journal of Steroid Biochemistry and Molecular Biology, 2018, 177, 159-170.	1.2	75
102	Reduced free-methionine in methionine-dependent SV40-transformed human fibroblasts synthesizing apparently normal amounts of methionine. Journal of Cellular Physiology, 1983, 117, 9-14.	2.0	74
103	Human and mouse hair follicles contain both multipotent and monopotent stem cells. Cell Cycle, 2009, 8, 176-177.	1.3	74
104	Methionine dependence in cancer cells $\hat{a} \in$ " A review. In Vitro, 1982, 18, 421-428.	1.2	73
105	Polyethylene Glycol Conjugation of Recombinant Methioninase for Cancer Therapy. Protein Expression and Purification, 1998, 12, 45-52.	0.6	73
106	<i>Salmonella</i> Promoters Preferentially Activated Inside Tumors. Cancer Research, 2008, 68, 4827-4832.	0.4	73
107	Tumor-selective, adenoviral-mediated GFP genetic labeling of human cancer in the live mouse reports future recurrence after resection. Cell Cycle, 2011, 10, 2737-2741.	1.3	73
108	Vemurafenib-resistant BRAF-V600E-mutated melanoma is regressed by MEK-targeting drug trametinib, but not cobimetinib in a patient-derived orthotopic xenograft (PDOX) mouse model. Oncotarget, 2016, 7, 71737-71743.	0.8	72

#	Article	IF	CITATIONS
109	Hair Follicle–Derived Blood Vessels Vascularize Tumors in Skin and Are Inhibited by Doxorubicin. Cancer Research, 2005, 65, 2337-2343.	0.4	71
110	Hand-held high-resolution fluorescence imaging system for fluorescence-guided surgery of patient and cell-line pancreatic tumors growing orthotopically in nude mice. Journal of Surgical Research, 2014, 187, 510-517.	0.8	71
111	A Genetically Engineered Oncolytic Adenovirus Decoys and Lethally Traps Quiescent Cancer Stem–like Cells in S/G2/M Phases. Clinical Cancer Research, 2013, 19, 6495-6505.	3.2	70
112	Glowing Tumors Make for Better Detection and Resection. Science Translational Medicine, 2011, 3, 110fs10.	5.8	69
113	Spatial–temporal FUCCI imaging of each cell in a tumor demonstrates locational dependence of cell cycle dynamics and chemoresponsiveness. Cell Cycle, 2014, 13, 2110-2119.	1.3	69
114	Selective efficacy of zoledronic acid on metastasis in a patientâ€derived orthotopic xenograph (PDOX) nudeâ€mouse model of human pancreatic cancer. Journal of Surgical Oncology, 2015, 111, 311-315.	0.8	69
115	Metastatic patterns of lung cancer visualized live and in process by green fluorescence protein expression. Clinical and Experimental Metastasis, 1997, 15, 547-552.	1.7	67
116	Facile whole-body imaging of internal fluorescent tumors in mice with an LED flashlight. BioTechniques, 2005, 39, 170-172.	0.8	67
117	Invading cancer cells are predominantly in G <sub>0</sub> /G <sub>1</sub> resulting in chemoresistance demonstrated by real-time FUCCI imaging. Cell Cycle, 2014, 13, 953-960.	1.3	67
118	Combination treatment with recombinant methioninase enables temozolomide to arrest a BRAF V600E melanoma in a patient-derived orthotopic xenograft (PDOX) mouse model. Oncotarget, 2017, 8, 85516-85525.	0.8	67
119	Chronologically-specific metastatic targeting of human pancreatic tumors in orthotopic models. Clinical and Experimental Metastasis, 2000, 18, 213-218.	1.7	66
120	Visualization of GFP-Expressing Tumors and Metastasis In Vivo. BioTechniques, 2001, 30, 1016-1026.	0.8	66
121	Synergistic Inhibitory Effect of Traditional Chinese Medicine Astragaloside IV and Curcumin on Tumor Growth and Angiogenesis in an Orthotopic Nude-Mouse Model of Human Hepatocellular Carcinoma. Anticancer Research, 2017, 37, 465-474.	0.5	66
122	Reversion to methionine independence by malignant rat and SV40-transformed human fibroblasts. Biochemical and Biophysical Research Communications, 1978, 82, 228-234.	1.0	65
123	Viable circulating metastatic cells produced in orthotopic but not ectopic prostate cancer models. Cancer Research, 2003, 63, 4239-43.	0.4	65
124	Extensive multi-organ metastasis following orthotopic onplantation of histologically-intact human bladder carcinoma tissue in nude mice. International Journal of Cancer, 1991, 49, 938-939.	2.3	64
125	Pharmacokinetics, Methionine Depletion, and Antigenicity of Recombinant Methioninase in Primates. Clinical Cancer Research, 2004, 10, 2131-2138.	3.2	64
126	Direct evidence that PTHrP expression promotes prostate cancer progression in bone. Biochemical and Biophysical Research Communications, 2005, 327, 468-472.	1.0	64

#	Article	IF	CITATIONS
127	Structure of the Antitumour Enzyme L-Methionine Â-Lyase from Pseudomonas putida at 1.8 A Resolution. Journal of Biochemistry, 2007, 141, 535-544.	0.9	64
128	Fluorescence-Guided Surgery Allows for More Complete Resection of Pancreatic Cancer, Resulting in Longer Disease-Free Survival Compared with Standard Surgery in Orthotopic Mouse Models. Journal of the American College of Surgeons, 2012, 215, 126-135.	0.2	64
129	Determination of clonality of metastasis by cell-specific color-coded fluorescent-protein imaging. Cancer Research, 2003, 63, 7785-90.	0.4	63
130	Patient-derived orthotopic xenograft (PDOX) nude mouse model of soft-tissue sarcoma more closely mimics the patient behavior in contrast to the subcutaneous ectopic model. Anticancer Research, 2015, 35, 697-701.	0.5	63
131	Imaging cancer dynamics inÂvivo at the tumor and cellular level with fluorescent proteins. Clinical and Experimental Metastasis, 2009, 26, 345-355.	1.7	61
132	Multiâ€color palette of fluorescent proteins for imaging the tumor microenvironment of orthotopic tumorgraft mouse models of clinical pancreatic cancer specimens. Journal of Cellular Biochemistry, 2012, 113, 2290-2295.	1.2	61
133	Antigen-Specific Bacterial Vaccine Combined with Anti-PD-L1 Rescues Dysfunctional Endogenous T Cells to Reject Long-Established Cancer. Cancer Immunology Research, 2013, 1, 123-133.	1.6	61
134	Orthotopic transplant mouse models with green fluorescent protein-expressing cancer cells to visualize metastasis and angiogenesis. Cancer and Metastasis Reviews, 1998, 17, 271-277.	2.7	60
135	Prediction of survival in patients with head and neck cancer using the histoculture drug response assay. Head and Neck, 2002, 24, 437-442.	0.9	60
136	Selective metastatic tumor labeling with green fluorescent protein and killing by systemic administration of telomerase-dependent adenoviruses. Molecular Cancer Therapeutics, 2009, 8, 3001-3008.	1.9	60
137	From hair to heart: nestin-expressing hair-follicle-associated pluripotent (HAP) stem cells differentiate to beating cardiac muscle cells. Cell Cycle, 2015, 14, 2362-2366.	1.3	60
138	Development of a high metastatic orthotopic model of human renal cell carcinoma in nude mice: benefits of fragment implantation compared to cell-suspension injection. Clinical and Experimental Metastasis, 1999, 17, 265-270.	1.7	59
139	The hair follicle as a gene therapy target. Nature Biotechnology, 2000, 18, 20-21.	9.4	59
140	Dual-Color Imaging of Nuclear-Cytoplasmic Dynamics, Viability, and Proliferation of Cancer Cells in the Portal Vein Area. Cancer Research, 2006, 66, 303-306.	0.4	59
141	Oral recombinant methioninase (o-rMETase) is superior to injectable rMETase and overcomes acquired gemcitabine resistance in pancreatic cancer. Cancer Letters, 2018, 432, 251-259.	3.2	59
142	Tumor-targetingSalmonella typhimuriumA1-R arrests growth of breast-cancer brain metastasis. Oncotarget, 2015, 6, 2615-2622.	0.8	59
143	In vivo efficacy of recombinant methioninase is enhanced by the combination of polyethylene glycol conjugation and pyridoxal 5'-phosphate supplementation. Cancer Research, 2003, 63, 8377-83.	0.4	59
144	Broad selective efficacy of recombinant methioninase and polyethylene glycol-modified recombinant methioninase on cancer cells In Vitro. Anticancer Research, 2010, 30, 1041-6.	0.5	59

#	Article	IF	CITATIONS
145	Topical liposome delivery of molecules to hair follicles in mice. Journal of Dermatological Science, 1997, 14, 101-108.	1.0	57
146	Mutant PIK3CA-Bearing Colon Cancer Cells Display Increased Metastasis in an Orthotopic Model. Cancer Research, 2007, 67, 5851-5858.	0.4	57
147	Fluorescence-guided surgery of human colon cancer increases complete resection resulting in cures in an orthotopic nude mouse model. Journal of Surgical Research, 2013, 179, 87-93.	0.8	57
148	Tumor-targeting Salmonella typhimurium A1-R combined with recombinant methioninase and cisplatinum eradicates an osteosarcoma cisplatinum-resistant lung metastasis in a patient-derived orthotopic xenograft (PDOX) mouse model: decoy, trap and kill chemotherapy moves toward the clinic. Cell Cycle, 2018, 17, 801-809.	1.3	57
149	Conversion of highly malignant colon cancer from an aggressive to a controlled disease by oral administration of a metalloproteinase inhibitor. Clinical and Experimental Metastasis, 1997, 15, 184-195.	1.7	56
150	High-level expression and bulk crystallization of recombinant l-methionine Î <sup>3</sup> -lyase, an anticancer agent. Applied Microbiology and Biotechnology, 2006, 70, 183-192.	1.7	56
151	Marker Expression in Circulating Cancer Cells of Pancreatic Cancer Patients. Journal of Surgical Research, 2011, 171, 631-636.	0.8	56
152	Recombinant methioninase in combination with doxorubicin (DOX) overcomes first-line DOX resistance in a patient-derived orthotopic xenograft nude-mouse model of undifferentiated spindle-cell sarcoma. Cancer Letters, 2018, 417, 168-173.	3.2	56
153	Near Infra-Red Photoimmunotherapy with Anti-CEA-IR700 Results in Extensive Tumor Lysis and a Significant Decrease in Tumor Burden in Orthotopic Mouse Models of Pancreatic Cancer. PLoS ONE, 2015, 10, e0121989.	1.1	56
154	Disruption of angiogenesis and tumor growth with an orally active drug that stabilizes the inactive state of PDGFRI <sup>2</sup> /B-RAF. Proceedings of the National Academy of Sciences of the United States of America, 2010, 107, 4299-4304.	3.3	55
155	Tumor-specific cell-cycle decoy by <i>Salmonella typhimurium</i> A1-R combined with tumor-selective cell-cycle trap by methioninase overcome tumor intrinsic chemoresistance as visualized by FUCCI imaging. Cell Cycle, 2016, 15, 1715-1723.	1.3	55
156	Promotion of tumor-associated macrophages infiltration by elevated neddylation pathway via NF-κB-CCL2 signaling in lung cancer. Oncogene, 2019, 38, 5792-5804.	2.6	55
157	Collective cancer invasion forms an integrin-dependent radioresistant niche. Journal of Experimental Medicine, 2020, 217, .	4.2	55
158	Intraperitoneal administration of tumor-targeting <i>Salmonella typhimurium</i> A1-R inhibits disseminated human ovarian cancer and extends survival in nude mice. Oncotarget, 2015, 6, 11369-11377.	0.8	55
159	A patient-like orthotopic implantation nude mouse model of highly metastatic human ovarian cancer. Clinical and Experimental Metastasis, 1998, 16, 751-756.	1.7	54
160	Advances in cellular, subcellular, and nanoscale imaging in vitro and in vivo. Cytometry Part A: the Journal of the International Society for Analytical Cytology, 2010, 77A, 667-676.	1.1	54
161	Development of the transgenic cyan fluorescent protein (CFP)â€expressing nude mouse for "Technicolor―cancer imaging. Journal of Cellular Biochemistry, 2009, 107, 328-334.	1.2	53
162	Protein-tyrosine Pseudokinase 7 (PTK7) Directs Cancer Cell Motility and Metastasis. Journal of Biological Chemistry, 2014, 289, 24238-24249.	1.6	53

#	Article	IF	CITATIONS
163	Tumor-Targeting <i>Salmonella typhimurium</i> A1-R Sensitizes Melanoma With a BRAF-V600E Mutation to Vemurafenib in a Patient-Derived Orthotopic Xenograft (PDOX) Nude Mouse Model. Journal of Cellular Biochemistry, 2017, 118, 2314-2319.	1.2	53
164	Surgical orthotopic implantation allows high lung and lymph node metastatic expression of human prostate carcinoma cell line PC-3 in nude mice. , 1998, 34, 169-174.		52
165	Patient-derived mouse models of cancer need to be orthotopic in order to evaluate targeted anti-metastatic therapy. Oncotarget, 2016, 7, 71696-71702.	0.8	52
166	Liposome targeting of high molecular weight DNA to the hair follicles of histocultured skin: A model for gene therapy of the hair growth processes. In Vitro Cellular & Developmental Biology, 1993, 29, 258-260.	1.0	50
167	Fluorescent LYVE-1 Antibody to Image Dynamically Lymphatic Trafficking of Cancer Cells In Vivo. Journal of Surgical Research, 2009, 151, 68-73.	0.8	50
168	An LED Light Source and Novel Fluorophore Combinations Improve Fluorescence Laparoscopic Detection of Metastatic Pancreatic Cancer in Orthotopic Mouse Models. Journal of the American College of Surgeons, 2012, 214, 997-1007e2.	0.2	50
169	The role of hair follicle nestinâ€expressing stem cells during whisker sensoryâ€nerve growth in longâ€term 3D culture. Journal of Cellular Biochemistry, 2013, 114, 1674-1684.	1.2	50
170	Tumor-targeting Salmonella typhimurium A1-R regresses an osteosarcoma in a patient-derived xenograft model resistant to a molecular-targeting drug. Oncotarget, 2017, 8, 8035-8042.	0.8	50
171	Oral Recombinant Methioninase Combined with Caffeine and Doxorubicin Induced Regression of a Doxorubicin-resistant Synovial Sarcoma in a PDOX Mouse Model. Anticancer Research, 2018, 38, 5639-5644.	0.5	50
172	The potential of nestin-expressing hair follicle stem cells in regenerative medicine. Expert Opinion on Biological Therapy, 2007, 7, 289-291.	1.4	49
173	Tumor-Targeting Salmonella typhimurium A1-R in Combination with Trastuzumab Eradicates HER-2-Positive Cervical Cancer Cells in Patient-Derived Mouse Models. PLoS ONE, 2015, 10, e0120358.	1.1	49
174	Intra-arterial administration of tumor-targeting <i>Salmonella typhimurium</i> A1-R regresses a cisplatin-resistant relapsed osteosarcoma in a patient-derived orthotopic xenograft (PDOX) mouse model. Cell Cycle, 2017, 16, 1164-1170.	1.3	49
175	Hypomethylation of hela cell DNA and the absence of 5-methylcytosine in SV40 and adenovirus (type 2) DNA: Analysis by HPLC. Biochemical and Biophysical Research Communications, 1982, 107, 19-26.	1.0	48
176	Skin histoculture assay for studying the hair cycle. In Vitro Cellular & Developmental Biology, 1992, 28, 695-698.	1.0	48
177	In vivo tumor delivery of the green fluorescent protein gene to report future occurrence of metastasis. Cancer Gene Therapy, 2000, 7, 1336-1340.	2.2	48
178	VEGF receptor antisense therapy inhibits angiogenesis and peritoneal dissemination of human gastric cancer in nude mice. Cancer Gene Therapy, 2002, 9, 197-201.	2.2	48
179	High Correlation of Whole-Body Red Fluorescent Protein Imaging and Magnetic Resonance Imaging on an Orthotopic Model of Pancreatic Cancer. Cancer Research, 2005, 65, 9829-9833.	0.4	48
180	UV light killing efficacy of fluorescent proteinâ€expressing cancer cells in vitro and in vivo. Journal of Cellular Biochemistry, 2010, 110, 1439-1446.	1.2	48

#	Article	IF	CITATIONS
181	A patient-derived orthotopic xenograft (PDOX) mouse model of a cisplatinum-resistant osteosarcoma lung metastasis that was sensitive to temozolomide and trabectedin: implications for precision oncology. Oncotarget, 2017, 8, 62111-62119.	0.8	48
182	Non-invasive fluorescent-protein imaging of orthotopic pancreatic-cancer-patient tumorgraft progression in nude mice. Anticancer Research, 2012, 32, 3063-7.	0.5	48
183	Product-delivering liposomes specifically target hair follicles in histocultured intact skin. In Vitro Cellular & Developmental Biology, 1992, 28, 679-681.	1.0	47
184	Real-time whole-body imaging of an orthotopic metastatic prostate cancer model expressing red fluorescent protein. Prostate, 2005, 62, 374-379.	1.2	47
185	Efficacy of tumor-targetingSalmonella typhimuriumA1-R on nude mouse models of metastatic and disseminated human ovarian cancer. Journal of Cellular Biochemistry, 2014, 115, n/a-n/a.	1.2	47
186	Determination of the optimal route of administration of Salmonella typhimurium A1-R to target breast cancer in nude mice. Anticancer Research, 2012, 32, 2501-8.	0.5	47
187	Real-Time In Vivo Green Fluorescent Protein Imaging of a Murine Leishmaniasis Model as a New Tool for Leishmania Vaccine and Drug Discovery. Vaccine Journal, 2008, 15, 1764-1770.	3.2	46
188	High-Throughput Screening for <i>Salmonella</i> Avirulent Mutants That Retain Targeting of Solid Tumors. Cancer Research, 2010, 70, 2165-2170.	0.4	46
189	Metronomic Gemcitabine in Combination with Sunitinib Inhibits Multisite Metastasis and Increases Survival in an Orthotopic Model of Pancreatic Cancer. Molecular Cancer Therapeutics, 2010, 9, 2068-2078.	1.9	46
190	Tumor-seeking Salmonella amino acid auxotrophs. Current Opinion in Biotechnology, 2011, 22, 917-923.	3.3	46
191	Ratiometric Activatable Cell-Penetrating Peptides Label Pancreatic Cancer, Enabling Fluorescence-Guided Surgery, Which Reduces Metastases and Recurrence in Orthotopic Mouse Models. Annals of Surgical Oncology, 2015, 22, 2082-2087.	0.7	46
192	Human Breast Cancer Cell Lines Co-Express Neuronal, Epithelial, and Melanocytic Differentiation Markers In Vitro and In Vivo. PLoS ONE, 2010, 5, e9712.	1.1	46
193	Cancer-cell killing by engineered Salmonella imaged by multiphoton tomography in live mice. Anticancer Research, 2012, 32, 4331-7.	0.5	46
194	Liposomes can specifically target entrapped melanin to hair follicles in histocultured skin. In Vitro Cellular & Developmental Biology, 1993, 29, 192-194.	1.0	45
195	An imageable highly metastatic orthotopic red fluorescent protein model of pancreatic cancer. Clinical and Experimental Metastasis, 2004, 21, 7-12.	1.7	45
196	In vivo imaging with fluorescent proteins: the new cell biology. Acta Histochemica, 2004, 106, 77-87.	0.9	45
197	Ovarian Tumor Attachment, Invasion, and Vascularization Reflect Unique Microenvironments in the Peritoneum: Insights from Xenograft and Mathematical Models. Frontiers in Oncology, 2013, 3, 97.	1.3	45
198	Targeting tumors with a killer-reporter adenovirus for curative fluorescence-guided surgery of soft-tissue sarcoma. Oncotarget, 2015, 6, 13133-13148.	0.8	45

#	Article	IF	CITATIONS
199	Optically imageable metastatic model of human breast cancer. Clinical and Experimental Metastasis, 2002, 19, 347-350.	1.7	44
200	Advantages of multi-color fluorescent proteins for whole-body and in vivo cellular imaging. Journal of Biomedical Optics, 2005, 10, 041202.	1.4	44
201	Orthotopic Metastatic (MetaMouse <sup><math display="inline">\hat{A}^{\otimes}</math></sup> ) Models for Discovery and Development of Novel Chemotherapy. , 2005, 111, 297-322.		44
202	Realâ€ŧime imaging of single cancerâ€cell dynamics of lung metastasis. Journal of Cellular Biochemistry, 2010, 109, 58-64.	1.2	44
203	Time-Course Imaging of Therapeutic Functional Tumor Vascular Normalization by Antiangiogenic Agents. Molecular Cancer Therapeutics, 2011, 10, 1173-1184.	1.9	44
204	Nestinâ€positive hair follicle pluripotent stem cells can promote regeneration of impinged peripheral nerve injury. Journal of Dermatology, 2012, 39, 33-38.	0.6	44
205	Tumor-Specific Fluorescence Antibody Imaging Enables Accurate Staging Laparoscopy in an Orthotopic Model of Pancreatic Cancer. Hepato-Gastroenterology, 2011, 59, 1994-9.	0.5	44
206	Efficacy of camptothecin analog DX-8951f (Exatecan Mesylate) on human pancreatic cancer in an orthotopic metastatic model. Cancer Research, 2003, 63, 80-5.	0.4	44
207	Histone methylation status of H3K4me3 and H3K9me3 under methionine restriction is unstable in methionine-addicted cancer cells, but stable in normal cells. Biochemical and Biophysical Research Communications, 2020, 533, 1034-1038.	1.0	43
208	Advantages of Fluorescence-Guided Laparoscopic Surgery of Pancreatic Cancer Labeled with Fluorescent Anti–Carcinoembryonic Antigen Antibodies in an Orthotopic Mouse Model. Journal of the American College of Surgeons, 2014, 219, 132-141.	0.2	42
209	Intravital microscopy of osteolytic progression and therapy response of cancer lesions in the bone. Science Translational Medicine, 2018, 10, .	5.8	42
210	Relevance of Vitamin D in Melanoma Development, Progression and Therapy. Anticancer Research, 2020, 40, 473-489.	0.5	42
211	Recombinant methioninase (rMETase) is an effective therapeutic for BRAF-V600E-negative as well as -positive melanoma in patient-derived orthotopic xenograft (PDOX) mouse models. Oncotarget, 2018, 9, 915-923.	0.8	42
212	Dual-Color-Coded Imaging of Viable Circulating Prostate Carcinoma Cells Reveals Genetic Exchange between Tumor Cells In Vivo, Contributing to Highly Metastatic Phenotypes. Cell Cycle, 2006, 5, 191-197.	1.3	41
213	Chemotherapy Targets the Hair-Follicle Vascular Network but Not the Stem Cells. Journal of Investigative Dermatology, 2007, 127, 11-15.	0.3	41
214	Current status and future perspectives of fluorescence-guided surgery for cancer. Expert Review of Anticancer Therapy, 2016, 16, 71-81.	1.1	41
215	Patient-derived orthotopic xenograft (PDOX) mouse model of adult rhabdomyosarcoma invades and recurs after resection in contrast to the subcutaneous ectopic model. Cell Cycle, 2017, 16, 91-94.	1.3	41
216	Methods for the development of tumor-targeting bacteria. Expert Opinion on Drug Discovery, 2014, 9, 741-750.	2.5	40

#	Article	IF	CITATIONS
217	Synergistic inhibition of autophagy and neddylation pathways as a novel therapeutic approach for targeting liver cancer. Oncotarget, 2015, 6, 9002-9017.	0.8	40
218	Tumor-Specific Labeling of Pancreatic Cancer Using a Humanized Anti-CEA Antibody Conjugated to a Near-Infrared Fluorophore. Annals of Surgical Oncology, 2018, 25, 1079-1085.	0.7	40
219	Targeting methionine with oral recombinant methioninase (o-rMETase) arrests a patient-derived orthotopic xenograft (PDOX) model of BRAF-V600E mutant melanoma: implications for chronic clinical cancer therapy and prevention. Cell Cycle, 2018, 17, 356-361.	1.3	40
220	A better fluorescent protein for whole-body imaging. Trends in Biotechnology, 2008, 26, 1-4.	4.9	39
221	Inhibition of spontaneous and experimental lung metastasis of soft-tissue sarcoma by tumor-targeting Salmonella typhimurium A1-R. Oncotarget, 2014, 5, 12849-12861.	0.8	39
222	An ultra-metastatic model of human colon cancer in nude mice. Clinical and Experimental Metastasis, 1999, 17, 51-58.	1.7	38
223	High-malignancy orthotopic nude mouse model of human prostate cancer LNCaP. , 1999, 39, 182-186.		38
224	Multipotent nestinâ€expressing hair follicle stem cells. Journal of Dermatology, 2009, 36, 1-9.	0.6	38
225	Tumor imaging with multicolor fluorescent protein expression. International Journal of Clinical Oncology, 2011, 16, 84-91.	1.0	38
226	Imaging the recruitment of cancerâ€associated fibroblasts by liverâ€metastatic colon cancer. Journal of Cellular Biochemistry, 2011, 112, 949-953.	1.2	38
227	Efficacy against lung metastasis with a tumor-targeting mutant of <i>Salmonella typhimurium</i> in immunocompetent mice. Cell Cycle, 2012, 11, 187-193.	1.3	38
228	The irony of highly-effective bacterial therapy of a patient-derived orthotopic xenograft (PDOX) model of Ewing's sarcoma, which was blocked by Ewing himself 80Âyears ago. Cell Cycle, 2017, 16, 1046-1052.	1.3	38
229	Oral dosing of Recombinant Methioninase Is Associated With a 70% Drop in PSA in a Patient With Bone-metastatic Prostate Cancer and 50% Reduction in Circulating Methionine in a High-stage Ovarian Cancer Patient. Anticancer Research, 2020, 40, 2813-2819.	0.5	38
230	Nestin-Expressing Stem Cells Promote Nerve Growth in Long-Term 3-Dimensional Gelfoam®-Supported Histoculture. PLoS ONE, 2013, 8, e67153.	1.1	38
231	The combination of temozolomide-irinotecan regresses a doxorubicin-resistant patient-derived orthotopic xenograft (PDOX) nude-mouse model of recurrent Ewing's sarcoma with a FUS-ERG fusion and <i>CDKN2A</i> deletion: Direction for third-line patient therapy. Oncotarget, 2017, 8, 103129-103136.	0.8	38
232	Imageable fluorescent metastasis resulting in transgenic GFP mice orthotopically implanted with human-patient primary pancreatic cancer specimens. Anticancer Research, 2012, 32, 1175-80.	0.5	38
233	Tumor Cells Genetically Labeled with GFP in the Nucleus and RFP in the Cytoplasm for Imaging Cellular Dynamics. Cell Cycle, 2006, 5, 1198-1201.	1.3	37
234	Watching stem cells in the skin of living mice noninvasively. Cell Cycle, 2011, 10, 2017-2020.	1.3	37

#	Article	IF	CITATIONS
235	In Vitro Culture and Characterization of Human Lung Cancer Circulating Tumor Cells Isolated by Size Exclusion from an Orthotopic Nude-Mouse Model Expressing Fluorescent Protein. Journal of Fluorescence, 2014, 24, 1531-1536.	1.3	37
236	Experimental Curative Fluorescence-guided Surgery of Highly Invasive Glioblastoma Multiforme Selectively Labeled With a Killer-reporter Adenovirus. Molecular Therapy, 2015, 23, 1182-1188.	3.7	37
237	<i>Salmonella typhimurium</i> A1-R targeting of a chemotherapy-resistant BRAF-V600E melanoma in a patient-derived orthotopic xenograft (PDOX) model is enhanced in combination with either vemurafenib or temozolomide. Cell Cycle, 2017, 16, 1288-1294.	1.3	37
238	MEK inhibitors cobimetinib and trametinib, regressed a gemcitabine-resistant pancreatic-cancer patient-derived orthotopic xenograft (PDOX). Oncotarget, 2017, 8, 47490-47496.	0.8	37
239	Whole-body imaging of bacterial infection and antibiotic response. Nature Protocols, 2006, 1, 2988-2994.	5.5	36
240	Multipotent nestin-expressing stem cells capable of forming neurons are located in the upper, middle and lower part of the vibrissa hair follicle. Cell Cycle, 2012, 11, 3513-3517.	1.3	36
241	Comparison of a chimeric anti-carcinoembryonic antigen antibody conjugated with visible or near-infrared fluorescent dyes for imaging pancreatic cancer in orthotopic nude mouse models. Journal of Biomedical Optics, 2013, 18, 126016.	1.4	36
242	Parathyroid Hormone Related-Protein Promotes Epithelial-to-Mesenchymal Transition in Prostate Cancer. PLoS ONE, 2014, 9, e85803.	1.1	36
243	Total-Homocysteine Enzymatic Assay. Clinical Chemistry, 2000, 46, 1686-1688.	1.5	35
244	Dual-Color Imaging of Nascent Blood Vessels Vascularizing Pancreatic Cancer in an Orthotopic Model Demonstrates Antiangiogenesis Efficacy of Gemcitabine. Journal of Surgical Research, 2006, 132, 164-169.	0.8	35
245	The Bisphosphonate Olpadronate Inhibits Skeletal Prostate Cancer Progression in a Green Fluorescent Protein Nude Mouse Model. Clinical Cancer Research, 2006, 12, 2602-2606.	3.2	35
246	An Imageable Metastatic Treatment Model of Nasopharyngeal Carcinoma. Clinical Cancer Research, 2007, 13, 3960-3967.	3.2	35
247	The advantages of hair follicle pluripotent stem cells over embryonic stem cells and induced pluripotent stem cells for regenerative medicine. Journal of Dermatological Science, 2010, 60, 131-137.	1.0	35
248	Hair follicle-associated-pluripotent (HAP) stem cells. Cell Cycle, 2017, 16, 2169-2175.	1.3	35
249	Efficacy of Recombinant Methioninase (rMETase) on Recalcitrant Cancer Patient-Derived Orthotopic Xenograft (PDOX) Mouse Models: A Review. Cells, 2019, 8, 410.	1.8	35
250	Improved Resection and Outcome of Colon-Cancer Liver Metastasis with Fluorescence-Guided Surgery Using In Situ GFP Labeling with a Telomerase-Dependent Adenovirus in an Orthotopic Mouse Model. PLoS ONE, 2016, 11, e0148760.	1.1	35
251	Intra-tumor L-methionine level highly correlates with tumor size in both pancreatic cancer and melanoma patient-derived orthotopic xenograft (PDOX) nude-mouse models. Oncotarget, 2018, 9, 11119-11125.	0.8	35
252	Solid tumors provide niche-specific conditions that lead to preferential growth of <i>Salmonella</i> . Oncotarget, 2016, 7, 35169-35180.	0.8	35

#	Article	IF	CITATIONS
253	Complementarity of ultrasound and fluorescence imaging in an orthotopic mouse model of pancreatic cancer. BMC Cancer, 2009, 9, 106.	1.1	34
254	High Efficacy of Pazopanib on an Undifferentiated Spindle-Cell Sarcoma Resistant to First-Line Therapy Is Identified With a Patient-Derived Orthotopic Xenograft (PDOX) Nude Mouse Model. Journal of Cellular Biochemistry, 2017, 118, 2739-2743.	1.2	34
255	Labeling the Stroma of a Patient-Derived Orthotopic Xenograft (PDOX) Mouse Model of Undifferentiated Pleomorphic Soft-Tissue Sarcoma With Red Fluorescent Protein for Rapid Non-Invasive Imaging for Drug Screening. Journal of Cellular Biochemistry, 2017, 118, 361-365.	1.2	34
256	Trabectedin and irinotecan combination regresses a cisplatinum-resistant osteosarcoma in a patient-derived orthotopic xenograft nude-mouse model. Biochemical and Biophysical Research Communications, 2019, 513, 326-331.	1.0	34
257	In Vivo Fluorescence Imaging Reveals the Promotion of Mammary Tumorigenesis by Mesenchymal Stromal Cells. PLoS ONE, 2013, 8, e69658.	1.1	34
258	Tumor-targeting <i>Salmonella typhimurium</i> A1-R prevents experimental human breast cancer bone metastasis in nude mice. Oncotarget, 2014, 5, 7119-7125.	0.8	34
259	Imaging tumor angiogenesis with fluorescent proteins. Apmis, 2004, 112, 441-449.	0.9	33
260	Effective Therapeutic Targeting of the Overexpressed HER-2 Receptor in a Highly Metastatic Orthotopic Model of Esophageal Carcinoma. Molecular Cancer Therapeutics, 2010, 9, 2037-2045.	1.9	33
261	Color-coded real-time cellular imaging of lung T-lymphocyte accumulation and focus formation in a mouse asthma model. Journal of Allergy and Clinical Immunology, 2010, 125, 461-468.e6.	1.5	33
262	Fluorescence laparoscopy imaging of pancreatic tumor progression in an orthotopic mouse model. Surgical Endoscopy and Other Interventional Techniques, 2011, 25, 48-54.	1.3	33
263	Multiphoton tomography visualizes collagen fibers in the tumor microenvironment that maintain cancerâ€cell anchorage and shape. Journal of Cellular Biochemistry, 2013, 114, 99-102.	1.2	33
264	In Vivo Fluorescence Imaging of Gastrointestinal Stromal Tumors Using Fluorophore-Conjugated Anti-KIT Antibody. Annals of Surgical Oncology, 2013, 20, 693-700.	0.7	33
265	Cancer cells mimic <i>in vivo</i> spatial-temporal cell-cycle phase distribution and chemosensitivity in 3-dimensional Gelfoam® histoculture but not 2-dimensional culture as visualized with real-time FUCCI imaging. Cell Cycle, 2015, 14, 808-819.	1.3	33
266	Temozolomide combined with irinotecan caused regression in an adult pleomorphic rhabdomyosarcoma patient-derived orthotopic xenograft (PDOX) nude-mouse model. Oncotarget, 2017, 8, 75874-75880.	0.8	33
267	Comparison of the selective targeting efficacy of <i>Salmonella typhimurium</i> A1-R and VNP20009 on the Lewis lung carcinoma in nude mice. Oncotarget, 2015, 6, 14625-14631.	0.8	33
268	Progression-free survival is accurately predicted in patients treated with chemotherapy for epithelial ovarian cancer by the histoculture drug response assay in a prospective correlative clinical trial at a single institution. Anticancer Research, 2013, 33, 1029-34.	0.5	33
269	Differential chemosensitivity of local and metastatic human gastric cancer after orthotopic transplantation of histologically intact tumor tissue in nude mice. International Journal of Cancer, 1993, 54, 397-401.	2.3	32
270	Development of a green fluorescent protein metastatic-cancer chick-embryo drug-screen model. Clinical and Experimental Metastasis, 2004, 21, 347-352.	1.7	32

#	Article	IF	CITATIONS
271	In vivo gene transfer between interacting human osteosarcoma cell lines is associated with acquisition of enhanced metastatic potential. Journal of Cellular Biochemistry, 2009, 108, 362-367.	1.2	32
272	Tumor-targeting amino acid auxotrophic Salmonella typhimurium. Amino Acids, 2009, 37, 509-521.	1.2	32
273	Direct transplantation of uncultured hairâ€follicle pluripotent stem (hfPS) cells promotes the recovery of peripheral nerve injury. Journal of Cellular Biochemistry, 2010, 110, 272-277.	1.2	32
274	Imaging the efficacy of UVC irradiation on superficial brain tumors and metastasis in live mice at the subcellular level. Journal of Cellular Biochemistry, 2013, 114, 428-434.	1.2	32
275	Fluorescence-guided surgery, but not bright-light surgery, prevents local recurrence in a pancreatic cancer patient derived orthotopic xenograft (PDOX) model resistant to neoadjuvant chemotherapy (NAC). Pancreatology, 2015, 15, 295-301.	0.5	32
276	The wayward methyl group and the cascade to cancer. Cell Cycle, 2017, 16, 825-829.	1.3	32
277	In vitro assays for chemotherapy sensitivity. Critical Reviews in Oncology/Hematology, 1993, 15, 99-111.	2.0	31
278	Use of histoculture and green fluorescent protein to visualize tumor cell host interaction. In Vitro Cellular and Developmental Biology - Animal, 1997, 33, 745-747.	0.7	31
279	Visualizing superficial human bladder cancer cell growth in vivo by green fluorescent protein expression. Cancer Gene Therapy, 2002, 9, 681-686.	2.2	31
280	Survival Efficacy of Adjuvant Cytosine-Analogue CS-682 in a Fluorescent Orthotopic Model of Human Pancreatic Cancer. Cancer Research, 2004, 64, 1828-1833.	0.4	31
281	Real-time confocal imaging of trafficking of nestin-expressing multipotent stem cells in mouse whiskers in long-term 3-D histoculture. In Vitro Cellular and Developmental Biology - Animal, 2012, 48, 301-305.	0.7	31
282	Stromal-cell and cancer-cell exosomes leading the metastatic exodus for the promised niche. Breast Cancer Research, 2013, 15, 310.	2.2	31
283	Nestin-Expressing Hair Follicle-Accessible Pluripotent Stem Cells for Nerve and Spinal Cord Repair. Cells Tissues Organs, 2014, 200, 42-47.	1.3	31
284	Isoproterenol directs hair follicle-associated pluripotent (HAP) stem cells to differentiate <i>in vitro</i> to cardiac muscle cells which can be induced to form beating heart-muscle tissue sheets. Cell Cycle, 2016, 15, 760-765.	1.3	31
285	Magnetic resonance and fluorescence-protein imaging of the anti-angiogenic and anti-tumor efficacy of selenium in an orthotopic model of human colon cancer. Anticancer Research, 2011, 31, 387-93.	0.5	31
286	The role of the intravascular microenvironment in spontaneous metastasis development. International Journal of Cancer, 2010, 126, 2534-2541.	2.3	30
287	Effective fluorescenceâ€guided surgery of liver metastasis using a fluorescent anti EA antibody. Journal of Surgical Oncology, 2016, 114, 951-958.	0.8	30
288	Combination of gemcitabine and docetaxel regresses both gastric leiomyosarcoma proliferation and invasion in an imageable patient-derived orthotopic xenograft (iPDOX) model. Cell Cycle, 2017, 16, 1063-1069.	1.3	30

#	Article	lF	CITATIONS
289	Growth of doxorubicinâ€resistant undifferentiated spindleâ€cell sarcoma PDOX is arrested by metabolic targeting with recombinant methioninase. Journal of Cellular Biochemistry, 2018, 119, 3537-3544.	1.2	30
290	Oral Recombinant Methioninase, Combined With Oral Caffeine and Injected Cisplatinum, Overcome Cisplatinum-Resistance and Regresses Patient-derived Orthotopic Xenograft Model of Osteosarcoma. Anticancer Research, 2019, 39, 4653-4657.	0.5	30
291	Selective antimetastatic activity of cytosine analog CS-682 in a red fluorescent protein orthotopic model of pancreatic cancer. Cancer Research, 2003, 63, 5521-5.	0.4	30
292	Homogeneous, Nonradioactive, Enzymatic Assay for Plasma Pyridoxal 5-Phosphate. Clinical Chemistry, 2002, 48, 1560-1564.	1.5	29
293	Precise navigation surgery of tumours in the lung in mouse models enabled by in situ fluorescence labelling with a killer-reporter adenovirus. BMJ Open Respiratory Research, 2015, 2, e000096.	1.2	29
294	Cell-cycle-dependent drug-resistant quiescent cancer cells induce tumor angiogenesis after chemotherapy as visualized by real-time FUCCI imaging. Cell Cycle, 2017, 16, 406-414.	1.3	29
295	Metabolic targeting with recombinant methioninase combined with palbociclib regresses a doxorubicin-resistant dedifferentiated liposarcoma. Biochemical and Biophysical Research Communications, 2018, 506, 912-917.	1.0	29
296	Efficacy of oral recombinant methioninase combined with oxaliplatinum and 5-fluorouracil on primary colon cancer in a patient-derived orthotopic xenograft mouse model. Biochemical and Biophysical Research Communications, 2019, 518, 306-310.	1.0	29
297	Unbalanced transmethylation and the perturbation of the differentiated state leading to cancer. BioEssays, 1990, 12, 163-166.	1.2	28
298	In Vivo Cell Biology of Cancer Cells Visualized with Fluorescent Proteins. Current Topics in Developmental Biology, 2005, 70, 121-144.	1.0	28
299	Complementary use of fluorescence and magnetic resonance imaging of metastatic esophageal cancer in a novel orthotopic mouse model. International Journal of Cancer, 2010, 126, 2671-2681.	2.3	28
300	Tumor-targeting Salmonella typhimurium A1-R is a highly effective general therapeutic for undifferentiated soft tissue sarcoma patient-derived orthotopic xenograft nude-mouse models. Biochemical and Biophysical Research Communications, 2018, 497, 1055-1061.	1.0	28
301	Pioglitazone, an agonist of PPARγ, reverses doxorubicin-resistance in an osteosarcoma patient-derived orthotopic xenograft model by downregulating P-glycoprotein expression. Biomedicine and Pharmacotherapy, 2019, 118, 109356.	2.5	28
302	Polyethylene Glycol (PEG) Linked to Near Infrared (NIR) Dyes Conjugated to Chimeric Anti-Carcinoembryonic Antigen (CEA) Antibody Enhances Imaging of Liver Metastases in a Nude-Mouse Model of Human Colon Cancer. PLoS ONE, 2014, 9, e97965.	1.1	27
303	Photoimmunotherapy lowers recurrence after pancreatic cancer surgery in orthotopic nude mouse models. Journal of Surgical Research, 2015, 197, 5-11.	0.8	27
304	Is DNA methylation the new guardian of the genome?. Molecular Cytogenetics, 2017, 10, 11.	0.4	27
305	Combination therapy of tumor-targeting Salmonella typhimurium A1-R and oral recombinant methioninase regresses a BRAF-V600E-negative melanoma. Biochemical and Biophysical Research Communications, 2018, 503, 3086-3092.	1.0	27
306	The combination of oral-recombinant methioninase and azacitidine arrests aÂchemotherapy-resistant osteosarcoma patient-derived orthotopic xenograft mouse model. Cancer Chemotherapy and Pharmacology, 2020, 85, 285-291.	1.1	27

#	Article	IF	CITATIONS
307	Measurement of androgen sensitivity in the human prostate in in vitro three-dimensional histoculture. Prostate, 1992, 21, 269-278.	1.2	26
308	Hair growth in vitro from histocultured skin. In Vitro Cellular & Developmental Biology, 1992, 28, 479-481.	1.0	26
309	Multi-organ metastatic capability of Chinese hamster ovary cells revealed by green fluorescent protein (GFP) expression. Clinical and Experimental Metastasis, 1999, 17, 417-422.	1.7	26
310	Real-time imaging of individual fluorescent-protein color-coded metastatic colonies in vivo. Clinical and Experimental Metastasis, 2003, 20, 633-638.	1.7	26
311	Automated Enzymatic Assay for Homocysteine. Clinical Chemistry, 2003, 49, 1029-1030.	1.5	26
312	Physicochemical and Pharmacokinetic Characterization of Highly Potent Recombinant l-Methionine Î <sup>3</sup> -Lyase Conjugated with Polyethylene Glycol as an Antitumor Agent. Cancer Research, 2006, 66, 2807-2814.	0.4	26
313	Color-Coded Fluorescent Protein Imaging of Angiogenesis: The AngioMouse® Models. Current Pharmaceutical Design, 2008, 14, 3810-3819.	0.9	26
314	Lentivirus-Based DsRed-2-Transfected Pancreatic Cancer Cells for Deep In Vivo Imaging of Metastatic Disease. Journal of Surgical Research, 2009, 157, 63-70.	0.8	26
315	Nestinâ€expressing interfollicular blood vessel network contributes to skin transplant survival and wound healing. Journal of Cellular Biochemistry, 2010, 110, 80-86.	1.2	26
316	Fluorescence-Guided Surgery in Combination with UVC Irradiation Cures Metastatic Human Pancreatic Cancer in Orthotopic Mouse Models. PLoS ONE, 2014, 9, e99977.	1.1	26
317	Comparison of Efficacy and Toxicity of Traditional Chinese Medicine (TCM) Herbal Mixture LQ and Conventional Chemotherapy on Lung Cancer Metastasis and Survival in Mouse Models. PLoS ONE, 2014, 9, e109814.	1.1	26
318	Fluorescence-guided surgery improves outcome in an orthotopic osteosarcoma nude-mouse model. Journal of Orthopaedic Research, 2014, 32, 1596-1601.	1.2	26
319	3â€Ðimensional Tissue Is Formed From Cancer Cells In Vitro on Gelfoam <sup>®</sup> , But Not on Matrigel <sup>TM</sup> . Journal of Cellular Biochemistry, 2014, 115, 1362-1367.	1.2	26
320	Reconstitution of a metastatic-resistant tumor microenvironment with cancer-associated fibroblasts enables metastasis. Cell Cycle, 2017, 16, 533-535.	1.3	26
321	Patient-Derived Orthotopic Xenograft (PDOX) Models of Melanoma. International Journal of Molecular Sciences, 2017, 18, 1875.	1.8	26
322	Oral Recombinant Methioninase Overcomes Colorectal-cancer Liver Metastasis Resistance to the Combination of 5-Fluorouracil and Oxaliplatinum in a Patient-derived Orthotopic Xenograft Mouse Model. Anticancer Research, 2019, 39, 4667-4671.	0.5	26
323	Clinical Studies of Methionine-Restricted Diets for Cancer Patients. Methods in Molecular Biology, 2019, 1866, 95-105.	0.4	26
324	In vivo tumor delivery of the green fluorescent protein gene to report future occurrence of metastasis. Cancer Gene Therapy, 2000, 7, 1336-1340.	2.2	26

#	Article	IF	CITATIONS
325	Circulating human prostate cancer cells from an orthotopic mouse model rapidly captured by immunomagnetic beads and imaged by GFP expression. Anticancer Research, 2011, 31, 1535-9.	0.5	26
326	Model of selective gene therapy of hair growth: Liposome targeting of the active lac-z gene to hair follicles of histocultured skin. In Vitro Cellular and Developmental Biology - Animal, 1995, 31, 11-13.	0.7	25
327	High efficiency genetic modification of hair follicles and growing hair shafts. Proceedings of the National Academy of Sciences of the United States of America, 2002, 99, 13120-13124.	3.3	25
328	Circulating Half-Life of PEGylated Recombinant Methioninase Holoenzyme Is Highly Dose Dependent on Cofactor Pyridoxal-5′-Phosphate. Cancer Research, 2004, 64, 5775-5778.	0.4	25
329	Paclitaxel nanosuspensions for targeted chemotherapy – nanosuspension preparation, characterization, and use. Pharmaceutical Development and Technology, 2014, 19, 438-453.	1.1	25
330	Cryopreservation of the Hair Follicle Maintains Pluripotency of Nestin-Expressing Hair Follicle-Associated Pluripotent Stem Cells. Tissue Engineering - Part C: Methods, 2015, 21, 825-831.	1.1	25
331	Realâ€Time GFP Intravital Imaging of the Differences in Cellular and Angiogenic Behavior of Subcutaneous and Orthotopic Nudeâ€Mouse Models of Human PCâ€3 Prostate Cancer. Journal of Cellular Biochemistry, 2016, 117, 2546-2551.	1.2	25
332	Combining Tumor-Selective Bacterial Therapy with <b><i>Salmonella typhimurium</i></b> A1-R and Cancer Metabolism Targeting with Oral Recombinant Methioninase Regressed an Ewing's Sarcoma in a Patient-Derived Orthotopic Xenograft Model. Chemotherapy, 2018, 63, 278-283.	0.8	25
333	Anti-carcinoembryonic antigen-related cell adhesion molecule antibody for fluorescence visualization of primary colon cancer and metastases in patient-derived orthotopic xenograft mouse models. Oncotarget, 2020, 11, 429-439.	0.8	25
334	Minimal liver resection strongly stimulates the growth of human colon cancer in the liver of nude mice. Clinical and Experimental Metastasis, 1999, 17, 497-500.	1.7	24
335	Real-time GFP imaging of spontaneous HT-1080 fibrosarcoma lung metastases. Clinical and Experimental Metastasis, 2003, 20, 181-185.	1.7	24
336	Visualization of xenotransplanted human rhabdomyosarcoma after transfection with red fluorescent protein. Journal of Pediatric Surgery, 2006, 41, 1369-1376.	0.8	24
337	Fluorescence-Guided Surgery and Fluorescence Laparoscopy for Gastrointestinal Cancers in Clinically-Relevant Mouse Models. Gastroenterology Research and Practice, 2013, 2013, 1-8.	0.7	24
338	Nanoparticle albumin-bound-paclitaxel: a limited improvement under the current therapeutic paradigm of pancreatic cancer. Expert Opinion on Pharmacotherapy, 2015, 16, 943-947.	0.9	24
339	Near-infrared–conjugated humanized anti-carcinoembryonic antigen antibody targets colon cancer in an orthotopic nude-mouse model. Journal of Surgical Research, 2017, 218, 139-143.	0.8	24
340	The development of fluorescence guided surgery for pancreatic cancer: from bench to clinic. Expert Review of Anticancer Therapy, 2018, 18, 651-662.	1.1	24
341	Sorafenib and Palbociclib Combination Regresses a Cisplatinum-resistant Osteosarcoma in a PDOX Mouse Model. Anticancer Research, 2019, 39, 4079-4084.	0.5	24
342	PPARÎ <sup>3</sup> Agonist Pioglitazone in Combination With Cisplatinum Arrests a Chemotherapy-resistant Osteosarcoma PDOX Model. Cancer Genomics and Proteomics, 2020, 17, 35-40.	1.0	24

#	Article	IF	CITATIONS
343	A novel anionic-phosphate-platinum complex effectively targets an undifferentiated pleomorphic sarcoma better than cisplatinum and doxorubicin in a patient-derived orthotopic xenograft (PDOX). Oncotarget, 2017, 8, 63353-63359.	0.8	24
344	Blockage of autophagy pathway enhances <i>Salmonella</i> tumor-targeting. Oncotarget, 2016, 7, 22873-22882.	0.8	24
345	Tumor-educated macrophages promote tumor growth and peritoneal metastasis in an orthotopic nude mouse model of human pancreatic cancer. In Vivo, 2012, 26, 565-9.	0.6	24
346	High lung-metastatic variant of human osteosarcoma cells, selected by passage of lung metastasis in nude mice, is associated with increased expression of α(v)β(3) integrin. Anticancer Research, 2013, 33, 3623-7.	0.5	24
347	Imaging the Interaction of Pancreatic Cancer and Stellate Cells in the Tumor Microenvironment during Metastasis. Anticancer Research, 2015, 35, 2545-51.	0.5	24
348	MUC1 Selectively Targets Human Pancreatic Cancer in Orthotopic Nude Mouse Models. PLoS ONE, 2015, 10, e0122100.	1.1	23
349	Cell-cycle fate-monitoring distinguishes individual chemosensitive and chemoresistant cancer cells in drug-treated heterogeneous populations demonstrated by real-time FUCCI imaging. Cell Cycle, 2015, 14, 621-629.	1.3	23
350	Tumor-Targeting Salmonella typhimurium A1-R: An Overview. Methods in Molecular Biology, 2016, 1409, 1-8.	0.4	23
351	Targeting altered cancer methionine metabolism with recombinant methioninase (rMETase) overcomes partial gemcitabine-resistance and regresses a patient-derived orthotopic xenograft (PDOX) nude mouse model of pancreatic cancer. Cell Cycle, 2018, 17, 868-873.	1.3	23
352	Tumorâ€Targeting <i>Salmonella typhimurium</i> A1â€R Promotes Tumoricidal CD8 <sup>+</sup> T Cell Tumor Infiltration and Arrests Growth and Metastasis in a Syngeneic Pancreaticâ€Cancer Orthotopic Mouse Model. Journal of Cellular Biochemistry, 2018, 119, 634-639.	1.2	23
353	Efficacy of glycogen synthase kinase-3β targeting against osteosarcoma via activation of β-catenin. Oncotarget, 2016, 7, 77038-77051.	0.8	23
354	Survival efficacy of the combination of the methioninase gene and methioninase in a lung cancer orthotopic model. Cancer Gene Therapy, 2000, 7, 332-338.	2.2	22
355	Cytotoxic synergism of methioninase in combination with 5-fluorouracil and folinic acid. Biochemical Pharmacology, 2001, 61, 867-876.	2.0	22
356	Upregulation of thrombospondin-1 and angiogenesis in an aggressive human pancreatic cancer cell line selected for high metastasis. Molecular Cancer Therapeutics, 2009, 8, 1779-1786.	1.9	22
357	Simultaneous colorâ€coded imaging to distinguish cancer "stemâ€like―and nonâ€stem cells in the same tumor. Journal of Cellular Biochemistry, 2010, 111, 1035-1041.	1.2	22
358	Photoimmunotherapy Inhibits Tumor Recurrence After Surgical Resection on a Pancreatic Cancer Patient-Derived Orthotopic Xenograft (PDOX) Nude Mouse Model. Annals of Surgical Oncology, 2015, 22, 1469-1474.	0.7	22
359	Advantages of patientâ€derived orthotopic mouse models and genetic reporters for developing fluorescenceâ€guided surgery. Journal of Surgical Oncology, 2018, 118, 253-264.	0.8	22
360	Combination Treatment With Sorafenib and Everolimus Regresses a Doxorubicin-resistant Osteosarcoma in a PDOX Mouse Model. Anticancer Research, 2019, 39, 4781-4786.	0.5	22

#	Article	IF	CITATIONS
361	Lowering and Stabilizing PSA Levels in Advanced-prostate Cancer Patients With Oral Methioninase. Anticancer Research, 2021, 41, 1921-1926.	0.5	22
362	Temozolomide combined with irinotecan regresses a cisplatinum-resistant relapsed osteosarcoma in a patient-derived orthotopic xenograft (PDOX) precision-oncology mouse model. Oncotarget, 2018, 9, 7774-7781.	0.8	22
363	Recombinant methioninase combined with doxorubicin (DOX) regresses a DOX-resistant synovial sarcoma in a patient-derived orthotopic xenograft (PDOX) mouse model. Oncotarget, 2018, 9, 19263-19272.	0.8	22
364	Fluorescent proteins enhance UVC PDT of cancer cells. Anticancer Research, 2012, 32, 4327-30.	0.5	22
365	"Decadose―Effects of Cisplatin on Squamous Cell Carcinoma of the Upper Aerodigestive Tract. I. Histoculture Experiments. Laryngoscope, 1996, 106, 32-36.	1.1	21
366	Visualization of nascent tumor angiogenesis in lung and liver metastasis by differential dual-color fluorescence imaging in nestin-linked-GFP mice. Clinical and Experimental Metastasis, 2007, 23, 315-322.	1.7	21
367	Dynamic color-coded fluorescence imaging of the cell-cycle phase, mitosis, and apoptosis demonstrates how caffeine modulates cisplatinum efficacy. Journal of Cellular Biochemistry, 2013, 114, 2454-2460.	1.2	21
368	Oral recombinant methioninase increases TRAIL receptor-2 expression to regress pancreatic cancer in combination with agonist tigatuzumab in an orthotopic mouse model. Cancer Letters, 2020, 492, 174-184.	3.2	21
369	Tumor-specific near-infrared nanobody probe rapidly labels tumors in an orthotopic mouse model of pancreatic cancer. Surgery, 2020, 168, 85-91.	1.0	21
370	GFP-fluorescence-guided UVC irradiation inhibits melanoma growth and angiogenesis in nude mice. Anticancer Research, 2010, 30, 3291-4.	0.5	21
371	Imaging tumor angiogenesis with fluorescent proteins. Apmis, 2004, 112, 441-9.	0.9	20
372	Imaging UVC-induced DNA damage response in models of minimal cancer. Journal of Cellular Biochemistry, 2013, 114, 2493-2499.	1.2	20
373	Prostate Cancer Heterogeneous High-Metastatic Multi-Organ-Colonizing Chemo-Resistant Variants Selected by Serial Metastatic Passage in Nude Mice Are Highly Enriched for Multinucleate Giant Cells. PLoS ONE, 2015, 10, e0140721.	1.1	20
374	Real-Time Determination of the Cell-Cycle Position of Individual Cells within Live Tumors Using FUCCI Cell-Cycle Imaging. Cells, 2018, 7, 168.	1.8	20
375	Double-negative T Cells Inhibit Proliferation and Invasion of Human Pancreatic Cancer Cells in Co-culture. Anticancer Research, 2019, 39, 5911-5918.	0.5	20
376	Pathological Validity of Using Near-infrared Fluorescence Imaging for Securing Surgical Margins During Liver Resection. Anticancer Research, 2020, 40, 3873-3882.	0.5	20
377	Cervical Cancer Patient-Derived Orthotopic Xenograft (PDOX) is Sensitive to Cisplatinum and Resistant to Nab-paclitaxel. Anticancer Research, 2017, 37, 61-66.	0.5	20
378	The camptothecin derivative CPT-11 inhibits angiogenesis in a dual-color imageable orthotopic metastatic nude mouse model of human colon cancer. Anticancer Research, 2007, 27, 713-8.	0.5	20

#	Article	IF	CITATIONS
379	Efficacy of the Chinese traditional medicinal herb Celastrus orbiculatus Thunb on human hepatocellular carcinoma in an orthothopic fluorescent nude mouse model. Anticancer Research, 2012, 32, 1213-20.	0.5	20
380	Imaging the Different Mechanisms of Prostate Cancer Cell-killing by Tumor-targeting Salmonella typhimurium A1-R. Anticancer Research, 2015, 35, 5225-9.	0.5	20
381	The activity of camptothecin analogues is enhanced in histocultures of human tumors and human tumor xenografts by modulation of extracellular pH. Cancer Chemotherapy and Pharmacology, 2003, 52, 253-261.	1.1	19
382	A Novel Alkylating Agent, Glufosfamide, Enhances the Activity of Gemcitabine In Vitro, In Vivo. Neoplasia, 2007, 9, 625-633.	2.3	19
383	Bugging Tumors. Cancer Discovery, 2012, 2, 588-590.	7.7	19
384	Comparison of UVB and UVC Effects on the DNA Damageâ€Response Protein 53BP1 in Human Pancreatic Cancer. Journal of Cellular Biochemistry, 2014, 115, 1724-1728.	1.2	19
385	MEK inhibitor trametinib in combination with gemcitabine regresses a patient-derived orthotopic xenograft (PDOX) pancreatic cancer nude mouse model. Tissue and Cell, 2018, 52, 124-128.	1.0	19
386	Detection of Metastasis in a Patient-derived Orthotopic Xenograft (PDOX) Model of Undifferentiated Pleomorphic Sarcoma with Red Fluorescent Protein. Anticancer Research, 2019, 39, 81-85.	0.5	19
387	Novel targets identified by integrated cancer-stromal interactome analysis of pancreatic adenocarcinoma. Cancer Letters, 2020, 469, 217-227.	3.2	19
388	Dual-color imaging of nascent angiogenesis and its inhibition in liver metastases of pancreatic cancer. Anticancer Research, 2006, 26, 3237-42.	0.5	19
389	Surgically-Induced Multi-organ Metastasis in an Orthotopic Syngeneic Imageable Model of 4T1 Murine Breast Cancer. Anticancer Research, 2015, 35, 4641-6.	0.5	19
390	Surgical and Oncological Factors Affecting the Successful Engraftment of Patient-derived Xenografts in Pancreatic Ductal Adenocarcinoma. Anticancer Research, 2016, 36, 517-21.	0.5	19
391	A simultaneous colorimetric assay of free and protein-coupled polyethylene glycol. Analytical Biochemistry, 2003, 313, 335-337.	1.1	18
392	Dual-color, whole-body imaging in mice. Nature Biotechnology, 2005, 23, 790-790.	9.4	18
393	Imaging In Mice With Fluorescent Proteins: From Macro To Subcellular. Sensors, 2008, 8, 1157-1173.	2.1	18
394	InÂvivo serial selection of human pancreatic cancer cells in orthotopic mouse models produces high metastatic variants irrespective of Kras status. Journal of Surgical Research, 2013, 184, 290-298.	0.8	18
395	Back to the Future: Are Tumor-Targeting Bacteria the Next-Generation Cancer Therapy?. Methods in Molecular Biology, 2015, 1317, 239-260.	0.4	18
396	Eradication of osteosarcoma by fluorescence-guided surgery with tumor labeling by a killer-reporter adenovirus. Journal of Orthopaedic Research, 2016, 34, 836-844.	1.2	18

#	Article	IF	CITATIONS
397	Human hair-follicle associated pluripotent (hHAP) stem cells differentiate to cardiac-muscle cells. Cell Cycle, 2017, 16, 95-99.	1.3	18
398	A combination of irinotecan/cisplatinum and irinotecan/temozolomide or tumor-targeting Salmonella typhimurium A1-R arrest doxorubicin- and temozolomide-resistant myxofibrosarcoma in a PDOX mouse model. Biochemical and Biophysical Research Communications, 2018, 505, 733-739.	1.0	18
399	Tumor targeting <i>Salmonella typhimurium</i> A1-R in combination with gemcitabine (GEM) regresses partially GEM-resistant pancreatic cancer patient-derived orthotopic xenograft (PDOX) nude mouse models. Cell Cycle, 2018, 17, 2019-2026.	1.3	18
400	Doxorubicin-resistant pleomorphic liposarcoma with PDGFRA gene amplification is targeted and regressed by pazopanib in a patient-derived orthotopic xenograft mouse model. Tissue and Cell, 2018, 53, 30-36.	1.0	18
401	The Combination of Olaratumab with Doxorubicin and Cisplatinum Regresses a Chemotherapy-Resistant Osteosarcoma in a Patient-Derived Orthotopic Xenograft Mouse Model. Translational Oncology, 2019, 12, 1257-1263.	1.7	18
402	Hair-follicle-associated pluripotent stem cells derived from cryopreserved intact human hair follicles sustain multilineage differentiation potential. Scientific Reports, 2019, 9, 9326.	1.6	18
403	Efficacy of Tumor-Targeting Salmonella typhimurium A1-R against Malignancies in Patient-Derived Orthotopic Xenograft (PDOX) Murine Models. Cells, 2019, 8, 599.	1.8	18
404	Targeting neddylation inhibits intravascular survival and extravasation of cancer cells to prevent lung-cancer metastasis. Cell Biology and Toxicology, 2019, 35, 233-245.	2.4	18
405	Locally-applied 5-fluorouracil-loaded slow-release patch prevents pancreatic cancer growth in an orthotopic mouse model. Oncotarget, 2017, 8, 40140-40151.	0.8	18
406	The cyan fluorescent protein nude mouse as a host for multicolor-coded imaging models of primary and metastatic tumor microenvironments. Anticancer Research, 2012, 32, 31-8.	0.5	18
407	Color-coded real-time subcellular fluorescence imaging of the interaction between cancer and host cells in live mice. Anticancer Research, 2012, 32, 39-43.	0.5	18
408	The hair follicle and its stem cells as drug delivery targets. Expert Opinion on Drug Delivery, 2006, 3, 437-443.	2.4	17
409	Dual-Color Imaging of Angiogenesis and Its Inhibition in Bone and Soft Tissue Sarcoma. Journal of Surgical Research, 2007, 140, 165-170.	0.8	17
410	The preclinical discovery of bacterial therapy for the treatment of metastatic cancer with unique advantages. Expert Opinion on Drug Discovery, 2012, 7, 73-83.	2.5	17
411	Efficacy comparison of traditional Chinese medicine LQ versus gemcitabine in a mouse model of pancreatic cancer. Journal of Cellular Biochemistry, 2013, 114, 2131-2137.	1.2	17
412	Improved diseaseâ€free survival and overall survival after fluorescenceâ€guided surgery of liver metastasis in an orthotopic nude mouse model. Journal of Surgical Oncology, 2015, 112, 119-124.	0.8	17
413	A novel method for RNA extraction from FFPE samples reveals significant differences in biomarker expression between orthotopic and subcutaneous pancreatic cancer patient-derived xenografts. Oncotarget, 2017, 8, 5885-5894.	0.8	17
414	Oral recombinant methioninase combined with oxaliplatinum and 5-fluorouracil regressed a colon cancer growing on the peritoneal surface in a patient-derived orthotopic xenograft mouse model. Tissue and Cell, 2019, 61, 109-114.	1.0	17

#	Article	IF	CITATIONS
415	Pilot Phase I Clinical Trial of Methioninase on High-Stage Cancer Patients: Rapid Depletion of Circulating Methionine. Methods in Molecular Biology, 2019, 1866, 231-242.	0.4	17
416	Patient-derived orthotopic xenograft models of sarcoma. Cancer Letters, 2020, 469, 332-339.	3.2	17
417	The Experience of Greece as a Model to Contain COVID-19 Infection Spread. In Vivo, 2021, 35, 1285-1294.	0.6	17
418	A rapid HPLC method for the measurement of ultra-low plasma methionine concentrations applicable to methionine depletion therapy. Anticancer Research, 2005, 25, 59-62.	0.5	17
419	Efficacy of dietary antioxidants combined with a chemotherapeutic agent on human colon cancer progression in a fluorescent orthotopic mouse model. Anticancer Research, 2009, 29, 2421-6.	0.5	17
420	Long-working-distance fluorescence microscope with high-numerical-aperture objectives for variable-magnification imaging in live mice from macro- to subcellular. Journal of Biomedical Optics, 2010, 15, 1.	1.4	16
421	Engineered mesenchymal stem-cell-sheets patches prevents postoperative pancreatic leakage in a rat model. Scientific Reports, 2018, 8, 360.	1.6	16
422	Color-coded Imaging of the Fate of Cancer-cell-derived Exosomes During Pancreatic Cancer Metastases in a Nude-mouse Model. Anticancer Research, 2019, 39, 4055-4060.	0.5	16
423	Eribulin Suppressed Cisplatinum- and Doxorubicin-resistant Recurrent Lung Metastatic Osteosarcoma in a Patient-derived Orthotopic Xenograft Mouse Model. Anticancer Research, 2019, 39, 4775-4779.	0.5	16
424	Regorafenib regressed a doxorubicin-resistant Ewing's sarcoma in a patient-derived orthotopic xenograft (PDOX) nude mouse model. Cancer Chemotherapy and Pharmacology, 2019, 83, 809-815.	1.1	16
425	FUCCI Real-Time Cell-Cycle Imaging as a Guide for Designing Improved Cancer Therapy: A Review of Innovative Strategies to Target Quiescent Chemo-Resistant Cancer Cells. Cancers, 2020, 12, 2655.	1.7	16
426	Oral Recombinant Methioninase Prevents Obesity in Mice on a High-fat Diet. In Vivo, 2020, 34, 489-494.	0.6	16
427	Fluorescence-guided surgery of a highly-metastatic variant of human triple-negative breast cancer targeted with a cancer-specific GFP adenovirus prevents recurrence. Oncotarget, 2016, 7, 75635-75647.	0.8	16
428	Toxicology and efficacy of tumor-targeting <i>Salmonella typhimurium</i> A1-R compared to VNP 20009 in a syngeneic mouse tumor model in immunocompetent mice. Oncotarget, 2017, 8, 54616-54628.	0.8	16
429	Effective Metabolic Targeting of Human Osteosarcoma Cells In Vitro and in Orthotopic Nude-mouse Models with Recombinant Methioninase. Anticancer Research, 2017, 37, 4807-4812.	0.5	16
430	Combination Efficacy of Astragalus membranaceus and Curcuma wenyujin at Different Stages of Tumor Progression in an Imageable Orthotopic Nude Mouse Model of Metastatic Human Ovarian Cancer Expressing Red Fluorescent Protein. Anticancer Research, 2015, 35, 3193-207.	0.5	16
431	Bone Marrow Mesenchymal Stem Cells Reverse Liver Damage in a Carbon Tetrachloride-induced Mouse Model of Chronic Liver Injury. In Vivo, 2016, 30, 187-93.	0.6	16
432	Isolation and Culture of Hair Follicle Pluripotent Stem (hfPS) Cells and Their Use for Nerve and Spinal Cord Regeneration. Methods in Molecular Biology, 2010, 585, 401-420.	0.4	15

#	Article	IF	CITATIONS
433	Imaging the inhibition by anti-β1 integrin antibody of lung seeding of single osteosarcoma cells in live mice. International Journal of Cancer, 2012, 131, 2027-2033.	2.3	15
434	The Tumor-Educated-Macrophage Increase of Malignancy of Human Pancreatic Cancer Is Prevented by Zoledronic Acid. PLoS ONE, 2014, 9, e103382.	1.1	15
435	Comparison of Nestinâ€Expressing Multipotent Stem Cells in the Tongue Fungiform Papilla and Vibrissa Hair Follicle. Journal of Cellular Biochemistry, 2014, 115, 1070-1076.	1.2	15
436	Analysis of Two Complementary Single-Gene Deletion Mutant Libraries of Salmonella Typhimurium in Intraperitoneal Infection of BALB/c Mice. Frontiers in Microbiology, 2015, 6, 1455.	1.5	15
437	Implanted hair-follicle-associated pluripotent (HAP) stem cells encapsulated in polyvinylidene fluoride membrane cylinders promote effective recovery of peripheral nerve injury. Cell Cycle, 2017, 16, 1927-1932.	1.3	15
438	Anti-Claudin-1 Conjugated to a Near-Infrared Fluorophore Targets Colon Cancer in PDOX MouseÂModels. Journal of Surgical Research, 2019, 242, 145-150.	0.8	15
439	Combination of oral recombinant methioninase and decitabine arrests a chemotherapy-resistant undifferentiated soft-tissue sarcoma patient-derived orthotopic xenograft mouse model. Biochemical and Biophysical Research Communications, 2020, 523, 135-139.	1.0	15
440	Fluorescence-guided hepatobiliary surgery with long and short wavelength fluorophores. Hepatobiliary Surgery and Nutrition, 2020, 9, 615-639.	0.7	15
441	Fluorescent humanized anti-CEA antibody specifically labels metastatic pancreatic cancer in a patient-derived orthotopic xenograft (PDOX) mouse model. Oncotarget, 2018, 9, 37333-37342.	0.8	15
442	Anti-metastatic Efficacy of Traditional Chinese Medicine (TCM) Ginsenoside Conjugated to a VEFGR-3 Antibody on Human Gastric Cancer in an Orthotopic Mouse Model. Anticancer Research, 2017, 37, 979-986.	0.5	15
443	TRAF6 regulates the signaling pathway influencing colorectal cancer function through ubiquitination mechanisms. Cancer Science, 2022, 113, 1393-1405.	1.7	15
444	Comparison of androgen-independent growth and androgen-dependent growth in BPH and cancer tissue from the same radical prostatectomies in sponge-gel matrix histoculture. , 1997, 31, 250-254.		14
445	GFP-expressing vascularization of Gelfoam® as a rapid in vivo assay of angiogenesis stimulators and inhibitors. BioTechniques, 2007, 42, 294-298.	0.8	14
446	Use of fluorescent proteins and color-coded imaging to visualize cancer cells with different genetic properties. Cancer and Metastasis Reviews, 2016, 35, 5-19.	2.7	14
447	Analysis of Stroma Labeling During Multiple Passage of a Sarcoma Imageable Patient-Derived Orthotopic Xenograft (iPDOX) in Red Fluorescent Protein Transgenic Nude Mice. Journal of Cellular Biochemistry, 2017, 118, 3367-3371.	1.2	14
448	Temozolomide regresses a doxorubicinâ€resistant undifferentiated spindleâ€cell sarcoma patientâ€derived orthotopic xenograft (PDOX): precisionâ€oncology nudeâ€mouse model matching the patient with effective therapy. Journal of Cellular Biochemistry, 2018, 119, 6598-6603.	1.2	14
449	Trabectedin arrests a doxorubicin-resistant PDGFRA-activated liposarcoma patient-derived orthotopic xenograft (PDOX) nude mouse model. BMC Cancer, 2018, 18, 840.	1.1	14
450	Tumor-targeting Salmonella typhimurium A1-R overcomes nab-paclitaxel resistance in a cervical cancer PDOX mouse model. Archives of Gynecology and Obstetrics, 2019, 299, 1683-1690.	0.8	14

#	Article	IF	CITATIONS
451	A patient-derived orthotopic xenograft (PDOX) nude-mouse model precisely identifies effective and ineffective therapies for recurrent leiomyosarcoma. Pharmacological Research, 2019, 142, 169-175.	3.1	14
452	Chronic Treatment of an Advanced Prostate-cancer Patient With Oral Methioninase Resulted in Long-term Stabilization of Rapidly Rising PSA Levels. In Vivo, 2021, 35, 2171-2176.	0.6	14
453	Oral-recombinant Methioninase Converts an Osteosarcoma from Docetaxel-resistant to -Sensitive in a Clinically-relevant Patient-derived Orthotopic-xenograft (PDOX) Mouse Model. Anticancer Research, 2021, 41, 1745-1751.	0.5	14
454	Development of a Clinically-Precise Mouse Model of Rectal Cancer. PLoS ONE, 2013, 8, e79453.	1.1	14
455	Genetic and metabolic comparison of orthotopic and heterotopic patient-derived pancreatic-cancer xenografts to the original patient tumors. Oncotarget, 2018, 9, 7867-7881.	0.8	14
456	Therapeutic efficacy of tumor-targeting <i>Salmonella typhimurium</i> A1-R on human colorectal cancer liver metastasis in orthotopic nude-mouse models. Oncotarget, 2015, 6, 31368-31377.	0.8	14
457	Fluorescence Molecular Targeting of Colon Cancer to Visualize the Invisible. Cells, 2022, 11, 249.	1.8	14
458	Methionine Restriction: Ready for Prime Time in the Cancer Clinic?. Anticancer Research, 2022, 42, 641-644.	0.5	14
459	Treatment of cancer cells with methioninase produces DNA hypomethylation and increases DNA synthesis. Cancer Research, 2002, 62, 4685-9.	0.4	14
460	Dynamic subcellular imaging of cancer cell mitosis in the brain of live mice. Anticancer Research, 2013, 33, 1367-71.	0.5	14
461	Single cell time-lapse imaging of focus formation by the DNA damage-response protein 53BP1 after UVC irradiation of human pancreatic cancer cells. Anticancer Research, 2013, 33, 1373-7.	0.5	14
462	Linkage of methionine addiction, histone lysine hypermethylation, and malignancy. IScience, 2022, 25, 104162.	1.9	14
463	Extent and Instability of Trimethylation of Histone H3 Lysine Increases With Degree of Malignancy and Methionine Addiction. Cancer Genomics and Proteomics, 2022, 19, 12-18.	1.0	14
464	Cimetidine: An inhibitor or promoter of tumor growth?. , 1999, 81, 835-838.		13
465	A Dual-Color Genetically Engineered Mouse Model for Multispectral Imaging of the Pancreatic Microenvironment. Pancreas, 2013, 42, 952-958.	0.5	13
466	Fluorescence-guided surgery of prostate cancer bone metastasis. Journal of Surgical Research, 2014, 192, 124-133.	0.8	13
467	Fluorescent-Antibody Targeting of Insulin-Like Growth Factor-1 Receptor Visualizes Metastatic Human Colon Cancer in Orthotopic Mouse Models. PLoS ONE, 2016, 11, e0146504.	1.1	13
468	Tumor relapse prevented by combining adoptive T cell therapy with Salmonella typhimurium. Oncolmmunology, 2016, 5, e1130207.	2.1	13

#	Article	IF	CITATIONS
469	Future of Bacterial Therapy of Cancer. Methods in Molecular Biology, 2016, 1409, 177-184.	0.4	13
470	Imaging the microenvironment of pancreatic cancer patient-derived orthotopic xenografts (PDOX) growing in transgenic nude mice expressing GFP, RFP, or CFP. Cancer Letters, 2016, 380, 349-355.	3.2	13
471	Hypoxia Enhances Differentiation of Hair Follicle-Associated-Pluripotent (HAP) Stem Cells to Cardiac-Muscle Cells. Journal of Cellular Biochemistry, 2017, 118, 554-558.	1.2	13
472	Individualized doxorubicin sensitivity testing of undifferentiated soft tissue sarcoma (USTS) in a patient-derived orthotopic xenograft (PDOX) model demonstrates large differences between patients. Cell Cycle, 2018, 17, 627-633.	1.3	13
473	Eribulin regresses a doxorubicinâ€resistant Ewing's sarcoma with a FUSâ€ERG fusion and CDKN2A―deletion in a patientâ€derived orthotopic xenograft (PDOX) nude mouse model. Journal of Cellular Biochemistry, 2018, 119, 967-972.	1.2	13
474	Antibiotic Usage Reduced Overall Survival by over 70% in Non-small Cell Lung Cancer Patients on Anti-PD-1 Immunotherapy. Anticancer Research, 2021, 41, 4985-4993.	0.5	13
475	Efficacy of intraâ€hepatectomy 5â€FU on recurrence and metastasis of human hepatocellular carcinoma in nude mice. International Journal of Cancer, 2001, 91, 231-235.	2.3	13
476	Adjuvant treatment with tumor-targeting <i>Salmonella typhimurium</i> A1-R reduces recurrence and increases survival after liver metastasis resection in an orthotopic nude mouse model. Oncotarget, 2015, 6, 41856-41862.	0.8	13
477	Osteosarcoma Patient-derived Orthotopic Xenograft (PDOX) Models Used to Identify Novel and Effective Therapeutics: A Review. Anticancer Research, 2021, 41, 5865-5871.	0.5	13
478	A rapid imageable in vivo metastasis assay for circulating tumor cells. Anticancer Research, 2011, 31, 3125-8.	0.5	13
479	Primer dosing of S. typhimurium A1-R potentiates tumor-targeting and efficacy in immunocompetent mice. Anticancer Research, 2013, 33, 97-102.	0.5	13
480	Intraoperative imaging of metastatic lymph nodes using a fluorophore-conjugated antibody in a HER2/neu-expressing orthotopic breast cancer mouse model. Anticancer Research, 2013, 33, 419-24.	0.5	13
481	[3] Green fluorescent protein to visualize cancer progression and metastasis. Methods in Enzymology, 1999, 302, 20-31.	0.4	12
482	Imaging of Nucleolar Dynamics During the Cell Cycle of Cancer Cells in Live Mice. Cell Cycle, 2007, 6, 2706-2708.	1.3	12
483	Recent Advances on In Vivo Imaging with Fluorescent Proteins. Methods in Cell Biology, 2008, 85, 485-495.	0.5	12
484	Color-coded imaging of splenocyte-pancreatic cancer cell interactions in the tumor microenvironment. Cell Cycle, 2008, 7, 2916-2921.	1.3	12
485	Embryonic development of hair follicle pluripotent stem (hfPS) cells. Medical Molecular Morphology, 2010, 43, 123-127.	0.4	12
486	Stem-like and non-stem human pancreatic cancer cells distinguished by morphology and metastatic behavior. Journal of Cellular Biochemistry, 2011, 112, 3549-3554.	1.2	12

#	Article	IF	CITATIONS
487	Cellular and Subcellular Imaging in Live Mice Using Fluorescent Proteins. Current Pharmaceutical Biotechnology, 2012, 13, 537-544.	0.9	12
488	Major liver resection stimulates stromal recruitment and metastasis compared with repeated minor resection. Journal of Surgical Research, 2012, 178, 280-287.	0.8	12
489	Tumor-targeting <i>Salmonella typhimurium</i> A1-R inhibits human prostate cancer experimental bone metastasis in mouse models. Oncotarget, 2015, 6, 31335-31343.	0.8	12
490	Color-coded intravital imaging demonstrates a transforming growth factor-β (TGF-β) antagonist selectively targets stromal cells in a human pancreatic-cancer orthotopic mouse model. Cell Cycle, 2017, 16, 1008-1014.	1.3	12
491	Strategies for In Vivo Imaging Using Fluorescent Proteins. Journal of Cellular Biochemistry, 2017, 118, 2571-2580.	1.2	12
492	Splenectomy is associated with an aggressive tumor growth pattern and altered host immunity in an orthotopic syngeneic murine pancreatic cancer model. Oncotarget, 2017, 8, 88827-88834.	0.8	12
493	Gemcitabine combined with docetaxel precisely regressed a recurrent leiomyosarcoma peritoneal metastasis in a patient-derived orthotopic xenograft (PDOX) model. Biochemical and Biophysical Research Communications, 2019, 509, 1041-1046.	1.0	12
494	Expression of anti-aging type-XVII collagen (COL17A1/BP180) in hair follicle-associated pluripotent (HAP) stem cells during differentiation. Tissue and Cell, 2019, 59, 33-38.	1.0	12
495	Altered Methionine Metabolism in Cancer Cells. Methods in Molecular Biology, 2019, 1866, 13-26.	0.4	12
496	NEDD8-conjugating enzyme UBC12 as a novel therapeutic target in esophageal squamous cell carcinoma. Signal Transduction and Targeted Therapy, 2020, 5, 123.	7.1	12
497	Response of Triple-negative Breast Cancer Liver Metastasis to Oral Recombinant Methioninase in a Patient-derived Orthotopic Xenograft (PDOX) Model. In Vivo, 2020, 34, 3163-3169.	0.6	12
498	Oral Methioninase Inhibits Recurrence in a PDOX Mouse Model of Aggressive Triple-negative Breast Cancer. In Vivo, 2020, 34, 2281-2286.	0.6	12
499	Oral Methioninase for Covid-19 Methionine-restriction Therapy. In Vivo, 2020, 34, 1593-1596.	0.6	12
500	Combination Methionine-methylation-axis Blockade: A Novel Approach to Target the Methionine Addiction of Cancer. Cancer Genomics and Proteomics, 2021, 18, 113-120.	1.0	12
501	Hair-Follicle-Associated Pluripotent (HAP) Stem Cells Can Extensively Differentiate to Tyrosine-Hydroxylase-Expressing Dopamine-Secreting Neurons. Cells, 2021, 10, 864.	1.8	12
502	High-resolution magnetic resonance imaging of the efficacy of the cytosine analogue 1-[2-C-cyano-2-deoxy-beta-D-arabino-pentofuranosyl]-N(4)-palmitoyl cytosine (CS-682) in a liver-metastasis athymic nude mouse model. Cancer Research, 2003, 63, 2477-82.	0.4	12
503	Real-time imaging of apoptosis induction of human breast cancer cells by the traditional Chinese medicinal herb tubeimu. Anticancer Research, 2012, 32, 2509-14.	0.5	12
504	Subcellular real-time imaging of the efficacy of temozolomide on cancer cells in the brain of live mice. Anticancer Research, 2013, 33, 103-6.	0.5	12

#	Article	IF	CITATIONS
505	Salmonella typhimurium A1-R tumor targeting in immunocompetent mice is enhanced by a traditional Chinese medicine herbal mixture. Anticancer Research, 2013, 33, 1837-43.	0.5	12
506	Specific tumor labeling enhanced by polyethylene glycol linkage of near infrared dyes conjugated to a chimeric anti-carcinoembryonic antigen antibody in a nude mouse model of human pancreatic cancer. Journal of Biomedical Optics, 2014, 19, 101504.	1.4	11
507	Osteosarcoma Cells Enhance Angiogenesis Visualized by Color oded Imaging in the In Vivo Gelfoam® Assay. Journal of Cellular Biochemistry, 2014, 115, 1490-1494.	1.2	11
508	Comparison of label-free and GFP multiphoton imaging of hair follicle-associated pluripotent (HAP) stem cells in mouse whiskers. Cell Cycle, 2015, 14, 3430-3433.	1.3	11
509	Aging hair follicles rejuvenated by transplantation to a young subcutaneous environment. Cell Cycle, 2016, 15, 1093-1098.	1.3	11
510	High-efficacy targeting of colon-cancer liver metastasis with <i>Salmonella typhimurium</i> A1-R via intra-portal-vein injection in orthotopic nude-mouse models. Oncotarget, 2017, 8, 19065-19073.	0.8	11
511	Tumor-targeting Salmonella typhimurium A1-R suppressed an imatinib-resistant gastrointestinal stromal tumor with c-kit exon 11 and 17 mutations. Heliyon, 2018, 4, e00643.	1.4	11
512	Patterns of sensitivity to a panel of drugs are highly individualised for undifferentiated/unclassified soft tissue sarcoma (USTS) in patient-derived orthotopic xenograft (PDOX) nude-mouse models. Journal of Drug Targeting, 2019, 27, 211-216.	2.1	11
513	Olaratumab combined with doxorubicin and ifosfamide overcomes individual doxorubicin and olaratumab resistance of an undifferentiated soft-tissue sarcoma in a PDOX mouse model. Cancer Letters, 2019, 451, 122-127.	3.2	11
514	Near-infrared photoimmunotherapy is effective treatment for colorectal cancer in orthotopic nude-mouse models. PLoS ONE, 2020, 15, e0234643.	1.1	11
515	Triple-Methyl Blockade With Recombinant Methioninase, Cycloleucine, and Azacitidine Arrests a Pancreatic Cancer Patient-Derived Orthotopic Xenograft Model. Pancreas, 2021, 50, 93-98.	0.5	11
516	An mTOR and VEGFR inhibitor combination arrests a doxorubicin resistant lung metastatic osteosarcoma in a PDOX mouse model. Scientific Reports, 2021, 11, 8583.	1.6	11
517	Fiveâ€day waterâ€only fasting decreased metabolicâ€syndrome risk factors and increased antiâ€aging biomarkers without toxicity in a clinical trial of normalâ€weight individuals. Clinical and Translational Medicine, 2021, 11, e502.	1.7	11
518	Rapid tumorâ€labeling kinetics with a siteâ€specific nearâ€infrared antiâ€CEA nanobody in a patientâ€derived orthotopic xenograft mouse model of colon cancer. Journal of Surgical Oncology, 2021, 124, 1121-1127.	0.8	11
519	Inhibition of growth and metastasis of triple-negative breast cancer targeted by Traditional Chinese Medicine Tubeimu in orthotopic mice models. Chinese Journal of Cancer Research: Official Journal of China Anti-Cancer Association, Beijing Institute for Cancer Research, 2018, 30, 112-121.	0.7	11
520	In Vivo Selection of Intermediately- and Highly- Malignant Variants of Triple-negative Breast Cancer in Orthotopic Nude Mouse Models. Anticancer Research, 2016, 36, 6273-6278.	0.5	11
521	Enhanced resection of orthotopic red-fluorescent-protein-expressing human glioma by fluorescence-guided surgery in nude mice. Anticancer Research, 2013, 33, 107-11.	0.5	11
522	Therapeutic Efficacy of the Traditional Chinese Medicine Baishaoqiwu on TNBS-induced Colitis is Associated with Down-regulation of the TLR4/MyD88/NF-κB Signaling Pathway. In Vivo, 2016, 30, 181-6.	0.6	11

#	Article	IF	CITATIONS
523	Stage IV Pancreatic Cancer Patient Treated With FOLFIRINOX Combined With Oral Methioninase: A Highly-Rare Case With Long-term Stable Disease. Anticancer Research, 2022, 42, 2567-2572.	0.5	11
524	Expression of prostate-specific antigen in human prostate specimens in in vitro three-dimensional histoculture. In Vitro Cellular & Developmental Biology, 1993, 29, 523-524.	1.0	10
525	A Novel Approach to Gene Therapy of Albino Hair In Histoculture with a Retroviral Streptomyces Tyrosinase Gene. Pigment Cell & Melanoma Research, 2000, 13, 345-351.	4.0	10
526	Syngeneic lymph-node-targeting model of green fluorescent protein-expressing Lewis lung carcinoma. Clinical and Experimental Metastasis, 2005, 21, 705-708.	1.7	10
527	<i>In vivo</i> realâ€time imaging of nuclearâ€cytoplasmic dynamics of dormancy, proliferation and death of cancer cells. Apmis, 2008, 116, 716-729.	0.9	10
528	Extended-working-distance multiphoton micromanipulation microscope for deep-penetration imaging in live mice and tissue. Journal of Biomedical Optics, 2009, 14, 024032.	1.4	10
529	High Antimetastatic Efficacy of MEN4901/T-0128, a Novel Camptothecin Carboxymethyldextran Conjugate. Journal of Surgical Research, 2011, 171, 684-690.	0.8	10
530	In Vivo Imaging of Pancreatic Cancer with Fluorescent Proteins in Mouse Models. Methods in Molecular Biology, 2012, 872, 51-67.	0.4	10
531	High accuracy of mesoscopic epi-fluorescence tomography for non-invasive quantitative volume determination of fluorescent protein-expressing tumours in mice. European Radiology, 2012, 22, 1955-1962.	2.3	10
532	Fluorescent Proteins as Visible In Vivo Sensors. Progress in Molecular Biology and Translational Science, 2013, 113, 389-402.	0.9	10
533	Temozolomide targets and arrests a doxorubicin-resistant follicular dendritic-cell sarcoma patient-derived orthotopic xenograft mouse model. Tissue and Cell, 2019, 58, 17-23.	1.0	10
534	Osimertinib Regresses an EGFR-Mutant Cisplatinum- Resistant Lung Adenocarcinoma Growing in the Brain in Nude Mice. Translational Oncology, 2019, 12, 640-645.	1.7	10
535	The combination of gemcitabine and nab-paclitaxel as a novel effective treatment strategy for undifferentiated soft-tissue sarcoma in a patient-derived orthotopic xenograft (PDOX) nude-mouse model. Biomedicine and Pharmacotherapy, 2019, 111, 835-840.	2.5	10
536	Hair-Follicle-Associated Pluripotent (HAP) Stem Cells Encapsulated on Polyvinylidene Fluoride Membranes (PFM) Promote Functional Recovery from Spinal Cord Injury. Stem Cell Reviews and Reports, 2019, 15, 59-66.	5.6	10
537	Humanized Anti–Tumor-Associated Glycoprotein–72 for Submillimeter Near-Infrared Detection of Colon Cancer in Metastatic Mouse Models. Journal of Surgical Research, 2020, 252, 16-21.	0.8	10
538	The Anti-oxidant Monoterpene <i>p</i> -Cymene Reduced the Occurrence of Colorectal Cancer in a Hyperlipidemia Rat Model by Reducing Oxidative Stress and Expression of Inflammatory Cytokines. Anticancer Research, 2021, 41, 1213-1218.	0.5	10
539	Tumor Imaging Technologies in Mouse Models. Methods in Molecular Biology, 2015, 1267, 321-348.	0.4	10
540	Epstein-Barr HR-1 Virion DNA Is Very Highly Methylated. Journal of Virology, 1983, 45, 482-483.	1.5	10

#	Article	IF	CITATIONS
541	Fluorescence-Guided Surgery of Retroperitoneal-Implanted Human Fibrosarcoma in Nude Mice Delays or Eliminates Tumor Recurrence and Increases Survival Compared to Bright-Light Surgery. PLoS ONE, 2015, 10, e0116865.	1.1	10
542	The disintegrin echistatin in combination with doxorubicin targets high-metastatic human osteosarcoma overexpressing αvβ3 integrin in chick embryo and nude mouse models. Oncotarget, 2016, 7, 87031-87036.	0.8	10
543	Targeting the insulin growth factor-1 receptor with fluorescent antibodies enables high resolution imaging of human pancreatic cancer in orthotopic mouse models. Oncotarget, 2016, 7, 18262-18268.	0.8	10
544	Visualizing portal vein metastatic trafficking to the liver with green fluorescent protein-expressing tumor cells. Anticancer Research, 2004, 24, 3699-702.	0.5	10
545	Color-coded Live Imaging of Heterokaryon Formation and Nuclear Fusion of Hybridizing Cancer Cells. Anticancer Research, 2016, 36, 3827-31.	0.5	10
546	Green fluorescent protein imaging of tumor cells in mice. Lab Animal, 2002, 31, 34-41.	0.2	10
547	Unchecked DNA synthesis and blocked cell division induced by methionine deprivation in a human prostate cancer cell line. In Vitro Cellular & Developmental Biology, 1993, 29, 359-361.	1.0	9
548	Whole-Body Fluorescence Imaging with Green Fluorescence Protein. , 2002, 183, 135-148.		9
549	Biological Ablation of Sentinel Lymph Node Metastasis in Submucosally Invaded Early Gastrointestinal Cancer. Molecular Therapy, 2015, 23, 501-509.	3.7	9
550	Eradication of melanoma <i>in vitro</i> and <i>in vivo</i> via targeting with a Killer-Red-containing telomerase-dependent adenovirus. Cell Cycle, 2017, 16, 1502-1508.	1.3	9
551	Regorafenib regresses an imatinib-resistant recurrent gastrointestinal stromal tumor (CIST) with a mutation in exons 11 and 17 of c-kit in a patient-derived orthotopic xenograft (PDOX) nude mouse model. Cell Cycle, 2018, 17, 722-727.	1.3	9
552	Moesin Up-regulation Is Associated with Enhanced Tumor Progression Imaged Non-invasively in an Orthotopic Mouse Model of Human Glioblastoma. Anticancer Research, 2018, 38, 3267-3272.	0.5	9
553	l-[Methyl-11C] Methionine-Positron-Emission Tomography (MET-PET). Methods in Molecular Biology, 2019, 1866, 267-271.	0.4	9
554	Tumor-Specific S/G2-Phase Cell Cycle Arrest of Cancer Cells by Methionine Restriction. Methods in Molecular Biology, 2019, 1866, 49-60.	0.4	9
555	Effective targeting of the ubiquitin-like modifier NEDD8 for lung adenocarcinoma treatment. Cell Biology and Toxicology, 2020, 36, 349-364.	2.4	9
556	<i>Brucea javanica</i> Increases Survival and Enhances Gemcitabine Efficacy in a Patient-derived Orthotopic Xenograft (PDOX) Mouse Model of Pancreatic Cancer. Anticancer Research, 2020, 40, 4969-4978.	0.5	9
557	Pazopanib Inhibits Tumor Growth, Lymph-node Metastasis and Lymphangiogenesis of an Orthotopic Mouse of Colorectal Cancer. Cancer Genomics and Proteomics, 2020, 17, 131-139.	1.0	9
558	Andrographolide Induces Noxa-Dependent Apoptosis by Transactivating ATF4 in Human Lung Adenocarcinoma Cells. Frontiers in Pharmacology, 2021, 12, 680589.	1.6	9

#	Article	IF	CITATIONS
559	Neddylation Regulates Macrophages and Implications for Cancer Therapy. Frontiers in Cell and Developmental Biology, 2021, 9, 681186.	1.8	9
560	Efficacy of YAP1-gene Knockdown to Inhibit Alveolar-Epithelial-Cell Senescence and Alleviate Idiopathic Pulmonary Fibrosis (IPF). Cancer Genomics and Proteomics, 2021, 18, 451-459.	1.0	9
561	Efficacy of Oral Recombinant Methioninase and Eribulin on a PDOX Model of Triple-negative Breast Cancer (TNBC) Liver Metastasis. In Vivo, 2021, 35, 2531-2534.	0.6	9
562	Adenoviral targeting of malignant melanoma for fluorescence-guided surgery prevents recurrence in orthotopic nude-mouse models. Oncotarget, 2016, 7, 18558-18572.	0.8	9
563	The combination of 5-FU, leucovorin and CPT-11 (FOLFIRI) prolongs survival through inhibition of metastasis in an orthotopic model of colon cancer. Anticancer Research, 2010, 30, 403-8.	0.5	9
564	Real-time imaging of $\hat{I}\pm v$ integrin molecular dynamics in osteosarcoma cells in vitro and in vivo. Anticancer Research, 2013, 33, 3021-5.	0.5	9
565	Decreased Expression of Tumor-suppressor Gene LKB1 Correlates with Poor Prognosis in Human Gastric Cancer. Anticancer Research, 2016, 36, 869-75.	0.5	9
566	Chapter 2 Color oded Fluorescent Mouse Models of Cancer Cell Interactions with Blood Vessels and Lymphatics. Methods in Enzymology, 2008, 445, 27-52.	0.4	8
567	Tumor-targeting Salmonella typhimurium A1-R overcomes partial carboplatinum-resistance of a cancer of unknown primary (CUP). Tissue and Cell, 2018, 54, 144-149.	1.0	8
568	Peritoneal Metastases in a Patient-derived Orthotopic Xenograft (PDOX) Model of Colon Cancer Imaged Non-invasively <i>via</i> Red Fluorescent Protein Labeled Stromal Cells. Anticancer Research, 2019, 39, 3463-3467.	0.5	8
569	TRAF6-Mediated Inflammatory Cytokines Secretion in LPS-induced Colorectal Cancer Cells Is Regulated by miR-140. Cancer Genomics and Proteomics, 2020, 17, 23-33.	1.0	8
570	A novel patient-derived orthotopic xenograft (PDOX) mouse model of highly-aggressive liver metastasis for identification of candidate effective drug-combinations. Scientific Reports, 2020, 10, 20105.	1.6	8
571	Co-implantation of Tumor and Extensive Surrounding Tissue Improved the Establishment Rate of Surgical Specimens of Human-Patient Cancer in Nude Mice: Toward the Goal of Universal Individualized Cancer Therapy. In Vivo, 2020, 34, 3241-3245.	0.6	8
572	A Triple-negative Matrix-producing Breast Carcinoma Patient-derived Orthotopic Xenograft (PDOX) Mouse Model Is Sensitive to Bevacizumab and Vinorelbine, Regressed by Eribulin and Resistant to Olaparib. Anticancer Research, 2020, 40, 2509-2514.	0.5	8
573	A review of tumor-specific fluorescence-guided surgery for colorectal cancer. Surgical Oncology, 2021, 36, 84-90.	0.8	8
574	The First Mouse Model of Primary Osteosarcoma of the Breast. In Vivo, 2021, 35, 1979-1983.	0.6	8
575	Real-Time Fluorescence Image-Guided Oncolytic Virotherapy for Precise Cancer Treatment. International Journal of Molecular Sciences, 2021, 22, 879.	1.8	8
576	Oral recombinant methioninase combined with paclitaxel arrests recalcitrant ovarian clear cell carcinoma growth in a patient-derived orthotopic xenograft (PDOX) nude-mouse model. Cancer Chemotherapy and Pharmacology, 2021, 88, 61-67.	1.1	8

#	Article	IF	CITATIONS
577	A Novel Color-Coded Liver Metastasis Mouse Model to Distinguish Tumor and Adjacent Liver Segment. Journal of Surgical Research, 2021, 264, 327-333.	0.8	8
578	Over-methylation of Histone H3 Lysines Is a Common Molecular Change Among the Three Major Types of Soft-tissue Sarcoma in Patient-derived Xenograft (PDX) Mouse Models. Cancer Genomics and Proteomics, 2021, 18, 715-721.	1.0	8
579	Andrographolide, a diterpene lactone from the Traditional Chinese Medicine Andrographis paniculate, induces senescence in human lung adenocarcinoma via p53/p21 and Skp2/p27. Phytomedicine, 2022, 98, 153933.	2.3	8
580	The cancer-inhibitory effects of proliferating tumor-residing fibroblasts. Biochimica Et Biophysica Acta: Reviews on Cancer, 2022, 1877, 188673.	3.3	8
581	Oral-recombinant Methioninase Converts an Osteosarcoma from Methotrexate-resistant to -sensitive in a Patient-derived Orthotopic-xenograft (PDOX) Mouse Model. Anticancer Research, 2022, 42, 731-737.	0.5	8
582	Inhibition of metastasis of circulating human prostate cancer cells in the chick embryo by an extracellular matrix produced by foreskin fibroblasts in culture. Anticancer Research, 2012, 32, 1573-7.	0.5	8
583	A color-coded imaging model of the interaction of αv integrin-GFP expressed in osteosarcoma cells and RFP expressing blood vessels in Gelfoam® vascularized in vivo. Anticancer Research, 2013, 33, 1361-6.	0.5	8
584	Early Reporting of Apoptosis by Real-time Imaging of Cancer Cells Labeled with Green Fluorescent Protein in the Nucleus and Red Fluorescent Protein in the Cytoplasm. Anticancer Research, 2015, 35, 2539-43.	0.5	8
585	Folate polyglutamate and monoglutamate accumulation in normal and SV40-transformed human fibroblasts. Journal of Cellular Physiology, 1981, 109, 497-505.	2.0	7
586	Imaging of the interaction of cancer cells and the lymphatic system. Advanced Drug Delivery Reviews, 2011, 63, 886-889.	6.6	7
587	Color oded Fluorescence Imaging of Lymphâ€Node Metastasis, Angiogenesis, and Its Drugâ€Induced Inhibition. Journal of Cellular Biochemistry, 2014, 115, 457-463.	1.2	7
588	Fluorescence-Guided Surgery of Liver Metastasis in Orthotopic Nude-Mouse Models. PLoS ONE, 2015, 10, e0138752.	1.1	7
589	Traditional Chinese medicine herbal mixture LQ arrests FUCCI-expressing HeLa cells in G0/G1 phase in 2D plastic, 2.5D Matrigel®, and 3D Gelfoam® culture visualized with FUCCI imaging. Oncotarget, 2015, 6, 5292-5298.	0.8	7
590	Fluorescenceâ€guided surgery of human prostate cancer experimental bone metastasis in nude mice using anti EA DyLight 650 for tumor illumination. Journal of Orthopaedic Research, 2016, 34, 559-565.	1.2	7
591	RT-PCR of peritoneal washings predicts peritoneal pancreatic cancer recurrence. Journal of Surgical Research, 2018, 226, 122-130.	0.8	7
592	3D Sponge-Matrix Histoculture: An Overview. Methods in Molecular Biology, 2018, 1760, 11-17.	0.4	7
593	Color-coded Imaging of the Circulating Tumor Cell Microenvironment. Anticancer Research, 2018, 38, 5635-5638.	0.5	7
594	Hair Follicle-Associated Pluripotent(HAP) Stem Cells. Progress in Molecular Biology and Translational Science, 2018, 160, 23-28.	0.9	7

#	Article	IF	CITATIONS
595	High-Mobility Group Box 1 expression predicts survival of patients after resection of adenocarcinoma of the ampulla of Vater. World Journal of Surgical Oncology, 2019, 17, 140.	0.8	7
596	Surgical and histological boundary of the hepatic hilar plate system: basic study relevant to surgery for hilar cholangiocarcinoma regarding the "true―proximal ductal margin. Journal of Hepato-Biliary-Pancreatic Sciences, 2019, 26, 159-168.	1.4	7
597	The combination of olaratumab with gemcitabine and docetaxel arrests a chemotherapy-resistant undifferentiated soft-tissue sarcoma in a patient-derived orthotopic xenograft mouse model. Cancer Chemotherapy and Pharmacology, 2019, 83, 1075-1082.	1.1	7
598	Adjuvant Oral Recombinant Methioninase Inhibits Lung Metastasis in a Surgical Breast-Cancer Orthotopic Syngeneic Model. Anticancer Research, 2020, 40, 4869-4874.	0.5	7
599	A Novel Anionic-phosphate-platinum Complex Effectively Targets a Cisplatinum-resistant Osteosarcoma in a Patient-derived Orthotopic Xenograft Mouse Model. Cancer Genomics and Proteomics, 2020, 17, 217-223.	1.0	7
600	Eribulin Regresses a Cisplatinum-resistant Rare-type Triple-negative Matrix-producing Breast Carcinoma Patient-derived Orthotopic Xenograft Mouse Model. Anticancer Research, 2020, 40, 2475-2479.	0.5	7
601	Exquisite Tumor Targeting by Salmonella A1-R in Combination with Caffeine and Valproic Acid Regresses an Adult Pleomorphic Rhabdomyosarcoma Patient-Derived Orthotopic Xenograft Mouse Model. Translational Oncology, 2020, 13, 393-400.	1.7	7
602	A Novel Procedure for Orthotopic Tibia Implantation for Establishment of a More Clinical Osteosarcoma PDOX Mouse Model. In Vivo, 2021, 35, 105-109.	0.6	7
603	Unique Benefits of Tumor-Specific Nanobodies for Fluorescence Guided Surgery. Biomolecules, 2021, 11, 311.	1.8	7
604	Tumor-targeting adenovirus OBP-401 inhibits primary and metastatic tumor growth of triple-negative breast cancer in orthotopic nude-mouse models. Oncotarget, 2016, 7, 85273-85282.	0.8	7
605	Non-toxic Efficacy of the Combination of Caffeine and Valproic Acid on Human Osteosarcoma Cells In Vitro and in Orthotopic Nude-mouse Models. Anticancer Research, 2016, 36, 4477-4482.	0.5	7
606	Real-time imaging of tumor progression in a fluorescent orthotopic mouse model of thyroid cancer. Anticancer Research, 2010, 30, 4415-22.	0.5	7
607	Comparative chemosensitivity of circulating human prostate cancer cells and primary cancer cells. Anticancer Research, 2012, 32, 2881-4.	0.5	7
608	siRNA Targeting of MDR1 Reverses Multidrug Resistance in a Nude Mouse Model of Doxorubicin-resistant Human Hepatocellular Carcinoma. Anticancer Research, 2016, 36, 2675-82.	0.5	7
609	In Vivo Isolation of a Highly-aggressive Variant of Triple-negative Human Breast Cancer MDA-MB-231 Using Serial Orthotopic Transplantation. Anticancer Research, 2016, 36, 3817-20.	0.5	7
610	Tumor Growth Control with IDO-Silencing <i>Salmonella</i> —Letter. Cancer Research, 2013, 73, 4591-4591.	0.4	6
611	Specific route mapping visualized with GFP of singleâ€file streaming contralateral and systemic metastasis of Lewis lung carcinoma cells beginning within hours of orthotopic implantion. Journal of Cellular Biochemistry, 2013, 114, 1738-1743.	1.2	6
612	Orthotopic Mouse Models of Tumor Metastasis Expressing Fluorescent Reporters Produce Imageable Circulating Tumor Cells. Cancer Microenvironment, 2014, 7, 133-138.	3.1	6

#	Article	IF	CITATIONS
613	Imaging Metastatic Cell Trafficking at the Cellular Level In Vivo with Fluorescent Proteins. Methods in Molecular Biology, 2014, 1070, 171-179.	0.4	6
614	Heterogeneous cell-cycle behavior in response to UVB irradiation by a population of single cancer cells visualized by time-lapse FUCCI imaging. Cell Cycle, 2015, 14, 1932-1937.	1.3	6
615	Nestin-Expressing Hair-Follicle-Associated Pluripotent (HAP) Stem Cells Promote Whisker Sensory-Nerve Growth in Long-Term 3D-Gelfoam® Histoculture. Methods in Molecular Biology, 2016, 1453, 39-47.	0.4	6
616	Peripheral-Nerve and Spinal-Cord Regeneration in Mice Using Hair-Follicle-Associated Pluripotent (HAP) Stem Cells. Methods in Molecular Biology, 2016, 1453, 21-32.	0.4	6
617	Early-age-dependent selective decrease of differentiation potential of hair-follicle-associated pluripotent (HAP) stem cells to beating cardiac-muscle cells. Cell Cycle, 2016, 15, 2619-2625.	1.3	6
618	Therapeutic Cellâ€Cycleâ€Decoy Efficacy of a Telomeraseâ€Dependent Adenovirus in an Orthotopic Model of Chemotherapyâ€Resistant Human Stomach Carcinomatosis Peritonitis Visualized With FUCCI Imaging. Journal of Cellular Biochemistry, 2017, 118, 3635-3642.	1.2	6
619	Tumorâ€targeting Salmonella typhimurium A1â€R arrests a doxorubicinâ€resistant PDGFRAâ€amplified patientâ€derived orthotopic xenograft mouse model of pleomorphic liposarcoma. Journal of Cellular Biochemistry, 2018, 119, 7827-7833.	1.2	6
620	Tumor-sealing Surgical Orthotopic Implantation of Human Colon Cancer in Nude Mice Induces Clinically-relevant Metastases Without Early Peritoneal Carcinomatosis. Anticancer Research, 2019, 39, 4065-4071.	0.5	6
621	Induction of Metastasis by Low-dose Gemcitabine in a Pancreatic Cancer Orthotopic Mouse Model: An Opposite Effect of Chemotherapy. Anticancer Research, 2019, 39, 5339-5344.	0.5	6
622	Development of Recombinant Methioninase for Cancer Treatment. Methods in Molecular Biology, 2019, 1866, 107-131.	0.4	6
623	High Efficacy of Recombinant Methioninase on Patient-Derived Orthotopic Xenograft (PDOX) Mouse Models of Cancer. Methods in Molecular Biology, 2019, 1866, 149-161.	0.4	6
624	Indocyanine Green Labels an Orthotopic Nude-Mouse Model of Very-Early Colon-Cancer Liver Metastases. In Vivo, 2020, 34, 2277-2280.	0.6	6
625	Fluorophore-conjugated Helicobacter pylori recombinant membrane protein (HopQ) labels primary colon cancer and metastases in orthotopic mouse models by binding CEA-related cell adhesion molecules. Translational Oncology, 2020, 13, 100857.	1.7	6
626	The identification of candidate effective combination regimens for pancreatic cancer using the histoculture drug response assay. Scientific Reports, 2020, 10, 12004.	1.6	6
627	Osimertinib regressed an EGFR-mutant lung-adenocarcinoma bone-metastasis mouse model and increased long-term survival. Translational Oncology, 2020, 13, 100826.	1.7	6
628	Oral Recombinant Methioninase Sensitizes a Bladder Cancer Orthotopic Xenograft Mouse Model to Low-dose Cisplatinum and Prevents Metastasis. Anticancer Research, 2020, 40, 6083-6091.	0.5	6
629	A Single Low Dose of Eribulin Regressed a Highly Aggressive Triple-negative Breast Cancer in a Patient-derived Orthotopic Xenograft Model. Anticancer Research, 2020, 40, 2481-2485.	0.5	6
630	Fangchinoline Inhibits Human Esophageal Cancer by Transactivating ATF4 to Trigger Both Noxa-Dependent Intrinsic and DR5-Dependent Extrinsic Apoptosis. Frontiers in Oncology, 2021, 11, 666549.	1.3	6

#	Article	IF	CITATIONS
631	Hyperthermia generated by magnetic nanoparticles for effective treatment of disseminated peritoneal cancer in an orthotopic nude-mouse model. Cell Cycle, 2021, 20, 1122-1133.	1.3	6
632	Extensive Hair Shaft Growth after Mouse Whisker Follicle Isolation, Cryopreservation and Transplantation in Nude Mice. PLoS ONE, 2015, 10, e0145997.	1.1	6
633	Imaging the Role of Multinucleate Pancreatic Cancer Cells and Cancer-Associated Fibroblasts in Peritoneal Metastasis in Mouse Models. Anticancer Research, 2017, 37, 3435-3440.	0.5	6
634	Tumor-targeting Salmonella typhimurium A1-R Inhibits Osteosarcoma Angiogenesis in the In Vivo Gelfoam® Assay Visualized by Color-coded Imaging. Anticancer Research, 2018, 38, 159-164.	0.5	6
635	Color-coded imaging of spontaneous vessel anastomosis in vivo. Anticancer Research, 2013, 33, 3041-5.	0.5	6
636	Complementarity of variable-magnification and spectral-separation fluorescence imaging systems for noninvasive detection of metastasis and intravital detection of single cancer cells in mouse models. Anticancer Research, 2015, 35, 661-7.	0.5	6
637	Comparison of GFP-Expressing Imageable Mouse Models of Human Esophageal Squamous Cell Carcinoma Established in Various Anatomical Sites. Anticancer Research, 2015, 35, 4655-63.	0.5	6
638	Fluorescent Anti-CEA Nanobody for Rapid Tumor-Targeting and Imaging in Mouse Models of Pancreatic Cancer. Biomolecules, 2022, 12, 711.	1.8	6
639	Protein carboxyl amidation increases the potential extent of protein polyethylene glycol conjugation. Analytical Biochemistry, 2004, 330, 264-271.	1.1	5
640	Comment re: Preclinical Model of Spontaneous Melanoma Metastasis: Figure 1 Cancer Research, 2009, 69, 719-719.	0.4	5
641	Detection of Colon Cancer Metastases With Fluorescence Laparoscopy in Orthotopic Nude Mouse Models. Archives of Surgery, 2012, 147, 876-80.	2.3	5
642	Live Cell Imaging in Live Animals with Fluorescent Proteins. Methods in Enzymology, 2012, 506, 197-224.	0.4	5
643	Nestin-Expressing Stem Cells from the Hair Follicle Can Differentiate Into Motor Neurons and Reduce Muscle Atrophy after Transplantation to Injured Nerves. Tissue Engineering - Part A, 2013, 20, 131106060201007.	1.6	5
644	Extensive Hair-Shaft Elongation by Isolated Mouse Whisker Follicles in Very Long-Term Gelfoam® Histoculture. PLoS ONE, 2015, 10, e0138005.	1.1	5
645	Real Time Metastatic Route Tracking of Orthotopic PCâ€3â€GFP Human Prostate Cancer Using Intravital Imaging. Journal of Cellular Biochemistry, 2016, 117, 1027-1032.	1.2	5
646	Introduction to Hair-Follicle-Associated Pluripotent Stem Cells. Methods in Molecular Biology, 2016, 1453, 1-5.	0.4	5
647	Protocols for Cryopreservation of Intact Hair Follicle That Maintain Pluripotency of Nestin-Expressing Hair-Follicle-Associated Pluripotent (HAP) Stem Cells. Methods in Molecular Biology, 2016, 1453, 173-178.	0.4	5
648	Clinical Factors That Affect the Establishment of Soft Tissue Sarcoma Patient-Derived Orthotopic Xenografts: A University of California, Los Angeles, Sarcoma Program Prospective Clinical Trial. JCO Precision Oncology, 2017, 2017, 1-13.	1.5	5

#	Article	IF	CITATIONS
649	Color-coded Imaging Distinguishes Cancer Cells, Stromal Cells, and Recombinant Cancer-stromal Cells in the Tumor Microenvironment During Metastasis. Anticancer Research, 2018, 38, 4417-4423.	0.5	5
650	Patient-derived orthotopic xenograft models for cancer of unknown primary precisely distinguish chemotherapy, and tumor-targeting S. typhimurium A1-R is superior to first-line chemotherapy. Signal Transduction and Targeted Therapy, 2018, 3, 12.	7.1	5
651	Safety and Toxicity of Recombinant Methioninase and Polyethylene Glycol (PEG) Recombinant Methioninase in Primates. Methods in Molecular Biology, 2019, 1866, 211-229.	0.4	5
652	Sutureless Surgical Orthotopic Implantation Technique of Primary and Metastatic Cancer in the Liver of Mouse Models. In Vivo, 2020, 34, 3153-3157.	0.6	5
653	Reversion from Methionine Addiction to Methionine Independence Results in Loss of Tumorigenic Potential of Highly-malignant Lung-cancer Cells. Anticancer Research, 2021, 41, 641-643.	0.5	5
654	Immuno-hyperthermia effected by antibody-conjugated nanoparticles selectively targets and eradicates individual cancer cells. Cell Cycle, 2021, 20, 1221-1230.	1.3	5
655	Fertile Seed and Rich Soil. , 1997, , 127-144.		5
656	Nestin-Driven Green Fluorescent Protein as an Imaging Marker for Nascent Blood Vessels in Mouse Models of Cancer. Methods in Molecular Biology, 2011, 689, 183-204.	0.4	5
657	Disintegrin targeting of an αvβ3 integrin-over-expressing high-metastatic human osteosarcoma with echistatin inhibits cell proliferation, migration, invasion and adhesion in vitro. Oncotarget, 2016, 7, 46315-46320.	0.8	5
658	Choline-Deficient-Diet-Induced Fatty Liver Is A Metastasis-Resistant Microenvironment. Anticancer Research, 2017, 37, 3429-3434.	0.5	5
659	Common bile duct injection as a novel method for establishing red fluorescent protein (RFP)-expressing human pancreatic cancer in nude mice. JOP: Journal of the Pancreas, 2006, 7, 193-9.	1.5	5
660	Imaging nuclear - cytoplasm dynamics of cancer cells in the intravascular niche of live mice. Anticancer Research, 2013, 33, 4229-36.	0.5	5
661	Independence of cytotoxic drug sensitivity profiles and receptor subtype of invasive ductal breast carcinoma demonstrated by the histoculture drug response assay (HDRA). Anticancer Research, 2014, 34, 7197-201.	0.5	5
662	Fluorescent Anti-MUC5AC Brightly Targets Pancreatic Cancer in a Patient-derived Orthotopic Xenograft. In Vivo, 2022, 36, 57-62.	0.6	5
663	Orthotopic mouse models expressing fluorescent proteins for cancer drug discovery. Expert Opinion on Drug Discovery, 2010, 5, 851-866.	2.5	4
664	Fluorescent Orthotopic Mouse Model of Pancreatic Cancer. Journal of Visualized Experiments, 2016, , .	0.2	4
665	Realâ€Time In Vivo Confocal Fluorescence Imaging of Prostate Cancer Boneâ€Marrow Micrometastasis Development at the Cellular Level in Nude Mice. Journal of Cellular Biochemistry, 2016, 117, 2533-2537.	1.2	4
666	Potential of immunotherapy for sarcoma. Cancer, 2017, 123, 1488-1489.	2.0	4

#	Article	IF	CITATIONS
667	Enhanced Metastatic Recurrence Via Lymphatic Trafficking of a High-Metastatic Variant of Human Triple-Negative Breast Cancer After Surgical Resection in Orthotopic Nude Mouse Models. Journal of Cellular Biochemistry, 2017, 118, 559-569.	1.2	4
668	Regarding the applications of fusion-fluorescence imaging using indocyanine green in laparoscopic hepatectomy. Translational Gastroenterology and Hepatology, 2017, 2, 70-70.	1.5	4
669	Combination of Trabectedin With Oxaliplatinum and 5-Fluorouracil Arrests a Primary Colorectal Cancer in a Patient-derived Orthotopic Xenograft Mouse Model. Anticancer Research, 2019, 39, 5999-6005.	0.5	4
670	The combination of gemcitabine and docetaxel arrests a doxorubicin-resistant dedifferentiated liposarcoma in a patient-derived orthotopic xenograft model. Biomedicine and Pharmacotherapy, 2019, 117, 109093.	2.5	4
671	Methionine Restriction and Life-Span Extension. Methods in Molecular Biology, 2019, 1866, 263-266.	0.4	4
672	Combination of Trabectedin With Irinotecan, Leucovorin and 5-Fluorouracil Arrests Primary Colorectal Cancer in an Imageable Patient-derived Orthotopic Xenograft Mouse Model. Anticancer Research, 2019, 39, 6463-6470.	0.5	4
673	Imaging the interaction of α <sub>v</sub> integrinâ€GFP in osteosarcoma cells with RFPâ€expressing host stromal cells and tumorâ€scaffold collagen in the primary and metastatic tumor microenvironment. Journal of Cellular Biochemistry, 2019, 120, 283-289.	1.2	4
674	A Gemcitabine Plus 5-Fluorouracil Combination Inhibits Gastric-Cancer Liver Metastasis in a PDOX Model: A Novel Treatment Strategy. Anticancer Research, 2020, 40, 5393-5397.	0.5	4
675	Recombinant Methioninase Combined With Tumor-targeting <i>Salmonella typhimurium</i> A1-R Induced Regression in a PDOX Mouse Model of Doxorubicin-resistant Dedifferentiated Liposarcoma. Anticancer Research, 2020, 40, 2515-2523.	0.5	4
676	Temozolomide and Pazopanib Combined with FOLFOX Regressed a Primary Colorectal Cancer in a Patient-derived Orthotopic Xenograft Mouse Model. Translational Oncology, 2020, 13, 100739.	1.7	4
677	Multikinase-Inhibitor Screening in Drug-resistant Osteosarcoma Patient-derived Orthotopic Xenograft Mouse Models Identifies the Clinical Potential of Regorafenib. Cancer Genomics and Proteomics, 2021, 18, 637-643.	1.0	4
678	Eribulin Inhibits Osteosarcoma in a Clinically-accurate Bone-tumor-insertion PDOX Mouse Model. Anticancer Research, 2021, 41, 1779-1784.	0.5	4
679	Color-coded Imaging Enables Fluorescence-guided Surgery to Resect the Tumor Along with the Tumor Microenvironment in a Syngeneic Mouse Model of EL-4 Lymphoma. Anticancer Research, 2016, 36, 4443-4448.	0.5	4
680	Osteosarcoma of the Breast in a Patient Derived Orthotopic Xenograft (PDOX) Mouse Model Is Arrested by both Cisplatinum and Eribulin. In Vivo, 2021, 35, 3107-3110.	0.6	4
681	Fluorescence-guided Surgery with Splenic Preservation Prevents Tumor Recurrence in an Orthotopic Nude-mouse Model of Human Pancreatic Cancer. Anticancer Research, 2018, 38, 665-670.	0.5	4
682	Visualizing the Tumor Microenvironment by Color-coded Imaging in Orthotopic Mouse Models of Cancer. Anticancer Research, 2018, 38, 1847-1857.	0.5	4
683	The cyan fluorescent protein (CFP) transgenic mouse as a model for imaging pancreatic exocrine cells. JOP: Journal of the Pancreas, 2009, 10, 152-6.	1.5	4
684	Chronic spinal cord injury functionally repaired by direct implantation of encapsulated hair-follicle-associated pluripotent (HAP) stem cells in a mouse model: Potential for clinical regenerative medicine. PLoS ONE, 2022, 17, e0262755.	1.1	4

#	Article	IF	CITATIONS
685	Real-time subcellular imaging in live animals: new visible targets for cancer drug discovery. IDrugs: the Investigational Drugs Journal, 2006, 9, 632-5.	0.7	4
686	A Color-coded Imageable Syngeneic Mouse Model of Stromal-cell Recruitment by Metastatic Lymphoma. Anticancer Research, 2015, 35, 4647-54.	0.5	4
687	Indocyanine Green Labeling of Tumors in the Liver Recurring After Radiofrequency Ablation Enables Complete Resection by Fluorescence-guided Surgery. Anticancer Research, 2022, 42, 1345-1350.	0.5	4
688	Immune reactions in skin and hair follicle gene therapy. Molecular Therapy, 2003, 7, 294-295.	3.7	3
689	3-Deazaadenosine, a Stabilizer of Whole-Blood Homocysteine Content, Does Not Interfere with the Single-Enzyme Homocysteine Assay while Totally Inhibiting the Enzyme Conversion Homocysteine Immunoassay. Clinical Chemistry, 2004, 50, 1703-1704.	1.5	3
690	PEG-Methioninase. , 2003, 519, 69-79.		3
691	Development of New Spontaneous Metastatic Heterotopic Model of Lewis Lung Carcinoma Imaged by GFP Expression. Cancer Investigation, 2011, 29, 692-695.	0.6	3
692	Shedding (Killer) Light on Tumors. Seminars in Thoracic and Cardiovascular Surgery, 2012, 24, 235-237.	0.4	3
693	In vivo imaging of nuclearâ€cytoplasmic deformation and partition during cancer cell death due to immune rejection. Journal of Cellular Biochemistry, 2012, 113, 465-472.	1.2	3
694	Long-Term Extensive Ectopic Hair Growth on the Spinal Cord of Mice from Transplanted Whisker Follicles. PLoS ONE, 2015, 10, e0133475.	1.1	3
695	Cryopreservation of Hair-Follicle Associated Pluripotent (HAP) Stem Cells Maintains Differentiation and Hair-Growth Potential. Advances in Experimental Medicine and Biology, 2016, 951, 191-198.	0.8	3
696	GFP labeling kinetics of triple-negative human breast cancer by a killer-reporter adenovirus in 3D Gelfoam® histoculture. In Vitro Cellular and Developmental Biology - Animal, 2017, 53, 479-482.	0.7	3
697	High-metastatic triple-negative breast-cancer variants selected in vivo become chemoresistant in vitro. In Vitro Cellular and Developmental Biology - Animal, 2017, 53, 285-287.	0.7	3
698	The Advantages of Using Fluorescent Proteins for In Vivo Imaging. Current Protocols in Essential Laboratory Techniques, 2017, 15, 9.6.1.	2.6	3
699	Comparison of in vitro invasiveness of high- and low-metastatic triple-negative human breast cancer visualized by color-coded imaging. In Vitro Cellular and Developmental Biology - Animal, 2017, 53, 96-98.	0.7	3
700	Clinical Correlation of the Histoculture Drug Response Assay in Gastrointestinal Cancer. Methods in Molecular Biology, 2018, 1760, 61-72.	0.4	3
701	Clinical Correlation of the Histoculture Drug Response Assay for Head and Neck Cancer. Methods in Molecular Biology, 2018, 1760, 83-92.	0.4	3
702	Pazopanib regresses a doxorubicin-resistant synovial sarcoma in a patient-derived orthotopic xenograft mouse model. Tissue and Cell, 2019, 58, 107-111.	1.0	3

#	Article	IF	CITATIONS
703	Efficacy of Methionine-Restricted Diets on Cancers In Vivo. Methods in Molecular Biology, 2019, 1866, 75-81.	0.4	3
704	Is the Hoffman Effect for Methionine Overuse Analogous to the Warburg Effect for Glucose Overuse in Cancer?. Methods in Molecular Biology, 2019, 1866, 273-278.	0.4	3
705	Afterword: Oral Methioninase—Answer to Cancer and Fountain of Youth?. Methods in Molecular Biology, 2019, 1866, 311-322.	0.4	3
706	Dietary Methionine Restriction-Based Cancer Chemotherapy in Rodents. Methods in Molecular Biology, 2019, 1866, 83-94.	0.4	3
707	Ligation Method to Specifically Label a Liver Segment With Indocyanine Green in an Orthotopic Nude-Mouse Liver-Metastasis Model. In Vivo, 2020, 34, 3159-3162.	0.6	3
708	The future of tumour-specific fluorescence-guided surgery for pancreatic cancer. The Lancet Gastroenterology and Hepatology, 2020, 5, 715-717.	3.7	3
709	Eribulin Regresses a Doxorubicin-resistant Dedifferentiated Liposarcoma in a Patient-derived Orthotopic Xenograft Mouse Model. Cancer Genomics and Proteomics, 2020, 17, 351-358.	1.0	3
710	Overexpressed NEDD8 as a potential therapeutic target in esophageal squamous cell carcinoma. Cancer Biology and Medicine, 2021, 19, 504-517.	1.4	3
711	A Patient-Derived Orthotopic Xenograft Model of Gastroesophageal-Junction Adenocarcinoma Translated to the Clinic by Tumor-Targeting Fluorescent Antibodies to Carcinoembryonic-Antigen-Related Cell-Adhesion Molecules. In Vivo, 2021, 35, 1959-1963.	0.6	3
712	Exosome Transfer Between Pancreatic-cancer Cells Is Associated With Metastasis in a Nude-mouse Model. Anticancer Research, 2021, 41, 2829-2834.	0.5	3
713	Transgenic Nude Mice Ubiquitously Expressing Fluorescent Proteins for Color-Coded Imaging of the Tumor Microenvironment. Methods in Molecular Biology, 2014, 1194, 353-365.	0.4	3
714	Dual-Color Imaging of Tumor Angiogenesis. Methods in Molecular Biology, 2009, 515, 45-61.	0.4	3
715	Efficacy of a Cell-Cycle Decoying Killer Adenovirus on 3-D Gelfoam®-Histoculture and Tumor-Sphere Models of Chemo-Resistant Stomach Carcinomatosis Visualized by FUCCI Imaging. PLoS ONE, 2016, 11, e0162991.	1.1	3
716	Histone H3 lysine-trimethylation markers are decreased by recombinant methioninase and increased by methotrexate at concentrations which inhibit methionine-addicted osteosarcoma cell proliferation. Biochemistry and Biophysics Reports, 2021, 28, 101177.	0.7	3
717	Real-time Non-invasive Spectral Imaging of Orthotopic Red Fluorescent Protein-expressing Lung Tumor Growth in Nude Mice. Anticancer Research, 2015, 35, 3755-9.	0.5	3
718	Orthotopic Implantation of Intact Tumor Tissue Leads to Metastasis of OCUM-2MD3 Human Gastric Cancer in Nude Mice Visualized in Real Time by Intravital Fluorescence Imaging. Anticancer Research, 2016, 36, 2125-30.	0.5	3
719	Efficacy of intra-hepatectomy 5-FU on recurrence and metastasis of human hepatocellular carcinoma in nude mice. International Journal of Cancer, 2001, 91, 231-235.	2.3	2
720	Noninvasive imaging for evaluation of the systemic delivery of capsid-modified adenovirus in an orthotopic model of advanced lung cancer. Cancer, 2007, 109, 1213-1213.	2.0	2

#	Article	IF	CITATIONS
721	The use of transgenic fluorescent mouse strains, fluorescent protein coding vectors, and innovative imaging techniques in the life sciences. Cytometry Part A: the Journal of the International Society for Analytical Cytology, 2008, 73A, 490-491.	1.1	2
722	Use of GFP for in vivo imaging: concepts and misconceptions. , 2008, , .		2
723	Real-time in vivo cellular imaging of graft-versus-host disease and its reaction to immunomodulatory reagents. Immunology Letters, 2012, 144, 33-40.	1.1	2
724	Lentivirus-Based DsRed-2-Transfected Pancreatic Cancer Cells for Deep In Vivo Imaging of Metastatic Disease. Methods in Molecular Biology, 2012, 872, 69-83.	0.4	2
725	Colorâ€Coded Imaging of Breast Cancer Metastatic Niche Formation in Nude Mice. Journal of Cellular Biochemistry, 2015, 116, 2730-2734.	1.2	2
726	Genetic Recombination Between Stromal and Cancer Cells Results in Highly Malignant Cells Identified by Color oded Imaging in a Mouse Lymphoma Model. Journal of Cellular Biochemistry, 2017, 118, 4216-4221.	1.2	2
727	Clinical Usefulness of the Histoculture Drug Response Assay for Prostate Cancer and Benign Prostate Hypertrophy (BPH). Methods in Molecular Biology, 2018, 1760, 101-107.	0.4	2
728	In Vivo-Like Growth Patterns of Multiple Types of Tumors in Gelfoam® Histoculture. Methods in Molecular Biology, 2018, 1760, 19-28.	0.4	2
729	Clinical Usefulness of the Histoculture Drug Response Assay for Breast Cancer. Methods in Molecular Biology, 2018, 1760, 93-100.	0.4	2
730	In Vivo-Like Cell-Cycle Phase Distribution of Cancer Cells in Gelfoam® Histoculture Observed in Real Time by FUCCI Imaging. Methods in Molecular Biology, 2018, 1760, 109-123.	0.4	2
731	Development of the Histoculture Drug Response Assay (HDRA). Methods in Molecular Biology, 2018, 1760, 39-48.	0.4	2
732	Prospective Clinical Correlation of the Histoculture Drug Response Assay for Ovarian Cancer. Methods in Molecular Biology, 2018, 1760, 73-81.	0.4	2
733	Hair-Shaft Growth in Gelfoam® Histoculture of Skin and Isolated Hair Follicles. Methods in Molecular Biology, 2018, 1760, 133-144.	0.4	2
734	Choline-deficient-diet Decreases Fibroblasts in the Circulating Tumor Cell (CTC) Microenvironment. Anticancer Research, 2019, 39, 4061-4064.	0.5	2
735	Methioninase Cell-Cycle Trap Cancer Chemotherapy. Methods in Molecular Biology, 2019, 1866, 133-148.	0.4	2
736	Humanized Fluorescent Tumor-associated Glycoprotein-72 Antibody Selectively Labels Colon-cancer Liver Metastases in Orthotopic Mouse Models. In Vivo, 2020, 34, 2303-2307.	0.6	2
737	Color-Coded Imaging of Cancer and Stromal-Cell Interaction in the Pancreatic-Cancer Tumor Microenvironment (TME). Methods in Molecular Biology, 2021, 2224, 99-111.	0.4	2
738	Effective Tumor Targeting by EphA2-Agonist-Biotin-Streptavidin Conjugates. Molecules, 2021, 26, 3687.	1.7	2

Robert M Hoffman

#	Article	IF	CITATIONS
739	Indocyanine Green Fluorescence Image-guided Laparoscopic Hepatectomy Enabled Resection of a Tumor Invisible With Ultrasonography. Anticancer Research, 2021, 41, 3867-3869.	0.5	2
740	Traditional Chinese Medicine Xihuang Wan Inhibited Lewis Lung Carcinoma in a Syngeneic Model, Equivalent to Cytotoxic Chemotherapy, by Altering Multiple Signaling Pathways. In Vivo, 2021, 35, 2005-2014.	0.6	2
741	Cimetidine: An inhibitor or promoter of tumor growth?. International Journal of Cancer, 1999, 81, 835-838.	2.3	2
742	Orthotopic Metastatic Mouse Models of Prostate Cancer. Cancer Metastasis - Biology and Treatment, 2008, , 143-169.	0.1	2
743	Imageable Clinically Relevant Mouse Models of Metastasis. Methods in Molecular Biology, 2014, 1070, 141-170.	0.4	2
744	Fluorescent Angiogenesis Models Using Gelfoam® Implanted in Transgenic Mice Expressing Fluorescent Proteins. Methods in Molecular Biology, 2014, 1135, 213-222.	0.4	2
745	Salmonella typhimurium A1-R and Cell-Cycle Decoy Therapy of Cancer. Methods in Molecular Biology, 2016, 1409, 165-175.	0.4	2
746	A Mouse Model of Fluorescent Protein-expressing Disseminated Peritoneal Lymphoma for Fluorescence-guided Surgery. Anticancer Research, 2016, 36, 4483-4488.	0.5	2
747	Differential Organ-targeting and Cellular Characteristics of Metastatic Human Pancreatic Cancer Cell Lines in Mouse Models. Anticancer Research, 2018, 38, 1927-1935.	0.5	2
748	CHFR-Promoter-Methylation Status Is Predictive of Response to Irinotecan-based Systemic Chemotherapy in Advanced Colorectal Cancer. Anticancer Research, 2022, 42, 697-707.	0.5	2
749	The Use of Living Cancer Cells Expressing Green Fluorescent Protein in the Nucleus and Red Fluorescence Protein in the Cytoplasm for Real-time Confocal Imaging of Chromosome and Cytoplasmic Dynamics During Mitosis. Anticancer Research, 2015, 35, 2553-7.	0.5	2
750	Recruitment of Cancer-Associated Fibroblasts and Blood Vessels by Orthotopic Liver Tumors Imaged in Red Fluorescent Protein (RFP) Transgenic Nude Mice. Anticancer Research, 2015, 35, 5821-5.	0.5	2
751	Color-Coded Imaging of Syngeneic Orthotopic Malignant Lymphoma Interacting with Host Stromal Cells During Metastasis. Anticancer Research, 2016, 36, 1473-8.	0.5	2
752	Modified Liver Hanging Maneuver for En-bloc Right-sided Hepatectomy Combined with Total Caudate Lobectomy for Colon-Cancer Liver Metastasis and Hepatocellular Carcinoma. Anticancer Research, 2016, 36, 1729-35.	0.5	2
753	Use of αv Integrin Linked to Green Fluorescent Protein in Osteosarcoma Cells and Confocal Microscopy to Image Molecular Dynamics During Lung Metastasis in Nude Mice. Anticancer Research, 2016, 36, 3811-6.	0.5	2
754	Efficacy of the Combination of a PARP Inhibitor and UVC on Cancer Cells as Imaged by Focus Formation by the DNA Repair-related Protein 53BP1 Linked to Green Fluorescent Protein. Anticancer Research, 2016, 36, 3821-6.	0.5	2
755	Deletion of <i>MTAP</i> Highly Sensitizes Osteosarcoma Cells to Methionine Restriction With Recombinant Methioninase. Cancer Genomics and Proteomics, 2022, 19, 299-304.	1.0	2
756	Therapeutic targeting of tumors with imageable GFP-expressing Salmonella typhimurium auxotrophic		1

mutants., 2008,,.

#	Article	IF	CITATIONS
757	Subcellular Imaging In Vivo: The Next GFP Revolution. Methods in Molecular Biology, 2012, 872, 255-263.	0.4	1
758	Laparoscopic Fluorescence Imaging for Identification and Resection of Pancreatic and Hepatobiliary Cancer. Frontiers of Gastrointestinal Research, 2013, , 92-99.	0.1	1
759	Realâ€Time Fluorescence Imaging of the DNA Damage Repair Response During Mitosis. Journal of Cellular Biochemistry, 2015, 116, 661-666.	1.2	1
760	Drug exposure in a metastatic human lung adenocarcinoma cell line gives rise to cells with differing adhesion, proliferation, and gene expression: Implications for cancer chemotherapy. Molecular Medicine Reports, 2015, 12, 3236-3242.	1.1	1
761	Fluorescence-Guided Surgery: It Is the Cure That Matters. Journal of the American College of Surgeons, 2015, 220, 377-379.	0.2	1
762	Protocols for Efficient Differentiation of Hair Follicle-Associated Pluripotent (HAP) Stem Cells to Beating Cardiac Muscle Cells. Methods in Molecular Biology, 2016, 1453, 151-159.	0.4	1
763	Protocols for Gelfoam® Histoculture of Hair-Shaft-Producing Mouse Whisker Follicles Containing Nestin-GFP-Expressing Hair-Follicle-Associated Pluripotent (HAP) Stem Cells for Long Time Periods. Methods in Molecular Biology, 2016, 1453, 145-150.	0.4	1
764	Use of α <sub>v</sub> Integrin Linked to GFP to Image Molecular Dynamics in Trafficking Cancer ell Emboli. Journal of Cellular Biochemistry, 2017, 118, 26-30.	1.2	1
765	Why Patient-Derived Mouse Models Need to Be Orthotopic. Molecular and Translational Medicine, 2017, , 277-284.	0.4	1
766	Methionine Dependency Determination of Human Patient Tumors in Gelfoam® Histoculture. Methods in Molecular Biology, 2018, 1760, 125-131.	0.4	1
767	Fluorescent Proteins as Sensors for Cellular Behavior in Mice. Progress in Molecular Biology and Translational Science, 2018, 160, 29-45.	0.9	1
768	Recombinant Methioninase as a DNA Demethylation Agent. Methods in Molecular Biology, 2019, 1866, 279-284.	0.4	1
769	Total Methionine Restriction Treatment of Cancer. Methods in Molecular Biology, 2019, 1866, 163-171.	0.4	1
770	An Improved Encapsulation Method for Cryopreserving Hepatocytes for Functional Transplantation Using a Thermo-reversible Gelation Polymer. In Vivo, 2020, 34, 2309-2316.	0.6	1
771	A Non-invasive Imageable GFP-expressing Mouse Model of Orthotopic Human Bladder Cancer. In Vivo, 2020, 34, 3225-3231.	0.6	1
772	The Combination of Cisplatinum and Doxorubicin Regressed Primary Osteosarcoma of the Breast in a PDOX Mouse Model. Anticancer Research, 2021, 41, 4715-4718.	0.5	1
773	Angiomouse: Imageable Models of Angiogenesis. , 0, , 293-310.		1
774	Imaging of Angiogenesis In Vivo with Fluorescent Proteins. , 2005, , 37-45.		1

#	Article	IF	CITATIONS
775	<i>Salmonella typhimurium</i> A1-R Exquisitely Targets and Arrests a Matrix-producing Triple-negative Breast Carcinoma in a PDOX Model. In Vivo, 2021, 35, 3067-3071.	0.6	1
776	Color-Coded Imaging of the Tumor Microenvironment (TME) in Human Patient–Derived Orthotopic Xenograft (PDOX) Mouse Models. Advances in Experimental Medicine and Biology, 2021, 1329, 163-179.	0.8	1
777	Methods for Tumor Targeting with Salmonella typhimurium A1-R. Methods in Molecular Biology, 2016, 1409, 143-164.	0.4	1
778	Fluorescence-guided laparoscopic hepatectomy. Annals of Laparoscopic and Endoscopic Surgery, 2016, 1, 10-10.	0.5	1
779	High Incidence of Lymph-node Metastasis in a Pancreatic-cancer Patient-derived Orthotopic Xenograft (PDOX) NOG-Mouse Model. Anticancer Research, 2022, 42, 739-743.	0.5	1
780	Hair-follicle-associated pluripotent (HAP) stem cells differentiate into mature beating cardiomyocyte sheets on flexible substrates in vitro. Medical Molecular Morphology, 2022, 55, 248-257.	0.4	1
781	Protein carboxyl amidation increases the potential extent of protein polyethylene glycol conjugation. Analytical Biochemistry, 2004, 330, 264-264.	1.1	Ο
782	Multi-color fluorescence imaging of sub-cellular dynamics of cancer cells in live mice. , 2006, 6098, 84.		0
783	Whole-body subcellular multicolor imaging. , 2007, , .		0
784	Subcellular real-time in vivo imaging of intralymphatic and intravascular cancer-cell trafficking. Proceedings of SPIE, 2008, , .	0.8	0
785	Specific in vivo labeling with GFP retroviruses, lentiviruses, and adenoviruses for imaging. , 2008, , .		Ο
786	Noninvasive imaging in vivo with fluorescent proteins from centimeters to micrometers. Proceedings of SPIE, 2008, , .	0.8	0
787	Watching stem cells at work with a flexible multiphoton tomograph. Proceedings of SPIE, 2012, , .	0.8	0
788	Nestin-expressing multipotent hair follicle stem cells for regenerative medicine. Expert Review of Dermatology, 2013, 8, 19-26.	0.3	0
789	Discovery of HAP Stem Cells. Methods in Molecular Biology, 2016, 1453, 15-20.	0.4	0
790	Protocols for Ectopic Hair Growth from Transplanted Whisker Follicles on the Spinal Cord of Mice. Methods in Molecular Biology, 2016, 1453, 137-144.	0.4	0
791	Cervical Cancer PDOX Models. Molecular and Translational Medicine, 2017, , 125-132.	0.4	0
792	Use of Patient-Derived Orthotopic Xenografts (PDOX) to Evaluate Transformative Cancer Therapeutics. Molecular and Translational Medicine, 2017, , 183-192.	0.4	0

#	Article	IF	CITATIONS
793	Fluorescent Protein-Expressing Transgenic Nude Mice as Hosts for Patient Tumors. Molecular and Translational Medicine, 2017, , 193-206.	0.4	0
794	Fluorescence Imaging of Tumors in Human Patient-Derived Orthotopic Xenograft (PDOX) Mouse Models. Molecular and Translational Medicine, 2017, , 207-216.	0.4	0
795	The Use of Patient-Derived Orthotopic Xenograft (PDOX) Models to Develop Curative Fluorescence-Guided Surgery of Cancer. Molecular and Translational Medicine, 2017, , 217-226.	0.4	Ο
796	Synergy of Patient-Derived Orthotopic Xenografts (PDOX) Models and Molecular Profiling for Optimal Therapy. Molecular and Translational Medicine, 2017, , 245-250.	0.4	0
797	The Revival of Patient-Derived Xenograft Mouse Models of Cancer: Way Back to the Future. Molecular and Translational Medicine, 2017, , 7-12.	0.4	Ο
798	Techniques for Surgical Orthotopic Implantation of Human Tumors to Immunodeficient Mice. Molecular and Translational Medicine, 2017, , 71-78.	0.4	0
799	21 Non-invasive single-photon and multi-photon imaging of stem cells and cancer cells in mouse models. , 2018, , 411-424.		0
800	Imaging DNA Repair After UV Irradiation Damage of Cancer Cells in Gelfoam® Histoculture. Methods in Molecular Biology, 2018, 1760, 199-203.	0.4	0
801	Diagnosis and Pathological Analysis of Patient Cancers by Detection of Proliferating Cells in Gelfoam® Histoculture. Methods in Molecular Biology, 2018, 1760, 49-60.	0.4	0
802	Hair Follicle-Associated Pluripotent (HAP) Stem Cells in Gelfoam® Histoculture for Use in Spinal Cord Repair. Methods in Molecular Biology, 2018, 1760, 145-162.	0.4	0
803	Expression and Targeting of Tumor Markers in Gelfoam® Histoculture: Potential Individualized Assays for Immuno-Oncology. Methods in Molecular Biology, 2018, 1760, 29-37.	0.4	0
804	Comparison of "Dimensionality―of Cancer Cell Culture in Gelfoam® Histoculture and Matrigel. Methods in Molecular Biology, 2018, 1760, 205-214.	0.4	0
805	Nerve Growth and Interaction in Gelfoam® Histoculture: A Nervous System Organoid. Methods in Molecular Biology, 2018, 1760, 163-186.	0.4	0
806	Imaging the Governing Step of Metastasis in Gelfoam® Histoculture. Methods in Molecular Biology, 2018, 1760, 215-220.	0.4	0
807	Beating Heart Cells from Hair-Follicle-Associated Pluripotent (HAP) Stem Cells. Methods in Molecular Biology, 2018, 1842, 241-254.	0.4	0
808	Human Hair Follicle Associated-Pluripotent (hHAP) Stem Cells Differentiate to Cardiac Muscle Cells. Methods in Molecular Biology, 2018, 1879, 385-392.	0.4	0
809	Methioninase Gene Therapy. Methods in Molecular Biology, 2019, 1866, 173-197.	0.4	0
810	Linkage of Methionine Dependence and Other Features of Malignancy. Methods in Molecular Biology, 2019, 1866, 27-36.	0.4	0

#	Article	IF	CITATIONS
811	RE: "Intraoperative Near-infrared Imaging Can Identify Neoplasms and Aid in Real-time Margin Assessment During Pancreatic Resection― Annals of Surgery, 2019, 270, 21-22.	2.1	Ο
812	Ischemia reperfusion-induced metastasis is resistant to PPARÎ <sup>3</sup> agonist pioglitazone in a murine model of colon cancer. Scientific Reports, 2020, 10, 18565.	1.6	0
813	Comparison of the Efficacy of EGFR Tyrosine Kinase Inhibitors Erlotinib and Low-dose Osimertinib on a PC-9-GFP EGFR Mutant Non-small-cell Lung Cancer Growing in the Brain of Nude Mice. In Vivo, 2020, 34, 1027-1030.	0.6	0
814	Patient-Like Orthotopic Metastatic Models of Human Cancer. , 2004, , 183-212.		0
815	Multicolor Imaging with Fluorescent Proteins in Mice. Reviews in Fluorescence, 2010, , 277-301.	0.5	Ο
816	Fluorescent Metastatic Mouse Models of Pancreatic Cancer for Drug Discovery. , 2010, , 51-72.		0
817	Future Directions: The Known and Unknown Roles of Hair-Follicle Stem Cell Types. , 2010, , 233-238.		0
818	Imaging the Steps of Metastasis at the Macro and Cellular Level with Fluorescent Proteins in Real Time. , 2011, , 125-166.		0
819	Targeting Cancer with Amino-Acid Auxotroph Salmonella typhimurium A1-R. , 2012, , 209-223.		0
820	Fluorophore-Conjugated Chimeric Anti-CEA Antibodies for Fluorescence-Guided Surgery of Gastrointestinal (GI) Tumors. , 2015, , 209-222.		0
821	Eradication of soft-tissue sarcoma in a patient-derived orthotopic xenograft (PDOX) model by tumor-targeting <i>Salmonella typhimurium</i> A1-R in combination with doxorubicin Journal of Clinical Oncology, 2016, 34, 11068-11068.	0.8	Ο
822	Fluorescence-guided surgery using patient-derived orthotopic xenograft models of cancer. , 2020, , 59-74.		0
823	Comparison of fluorescence-labeling strategies of colon cancer for fluorescence-guided surgery of liver metastasis in orthotopic mouse models. , 2020, , 31-44.		0
824	Precise recurrence-free fluorescence-guided surgery with color-coded cancer and stromal cells in a patient-derived orthotopic xenograft model of pancreatic cancer. , 2020, , 115-123.		0
825	Efficacy of the combination of fluorescence-guided surgery and adjuvant therapy in orthotopic nude mouse models of cancer. , 2020, , 45-58.		0
826	Fluorescence-guided surgery for primary and metastatic bone tumors in orthotopic nude mouse models. , 2020, , 125-137.		0
827	Fluorescence-guided surgery improved long-term survival in orthotopic nude mouse models of cancer. , 2020, , 3-19.		0
828	Subcellular Imaging of Cancer Cells in Live Mice. , 2007, 411, 121-129.		0

828 Subcellular Imaging of Cancer Cells in Live Mice. , 2007, 411, 121-129.

#	Article	IF	CITATIONS
829	Imaging Nuclear-Cytoplasmic Dynamics in Primary and Metastatic Colon Cancer in Nude Mice. Anticancer Research, 2016, 36, 2113-7.	0.5	0
830	Determinative Structural Features Identified With Probe-based Confocal Endomicroscopy for the Accurate Diagnosis of Gallbladder Malignancy. Anticancer Research, 2022, 42, 67-73.	0.5	0
831	Title is missing!. , 2020, 15, e0234643.		0
832	Title is missing!. , 2020, 15, e0234643.		0
833	Title is missing!. , 2020, 15, e0234643.		0
834	Title is missing!. , 2020, 15, e0234643.		0
835	Title is missing!. , 2020, 15, e0234643.		0
836	Title is missing!. , 2020, 15, e0234643.		0
837	ATR inhibition sensitizes liposarcoma to doxorubicin by increasing DNA damage American Journal of Cancer Research, 2022, 12, 1577-1592.	1.4	0